Inorg. Chem. **2009**, *48*, 2316−2332

A ^{13}C and ^{15}N Solid-State NMR Study of Structural Disorder and Aurophilic Bonding in Au^{I} and Au^{III} Cyanide Complexes

Kristopher J. Harris and Roderick E. Wasylishen*

Department of Chemistry, University of Alberta, Edmonton, Alberta, T6G 2G2, Canada

Received November 19, 2008

Solid-state nuclear magnetic resonance has been used to study several cyanoaurates. Carbon-13 and nitrogen-15 NMR spectra of samples enriched with isotopically labeled ^{13}C,^{15}N cyanide ligands were recorded for stationary samples and samples spinning at the magic angle. Several salts of the dicyanoaurate(I) anion, $M[Au(CN)_2]$, where M = *n*-butylammonium, potassium, and thallium, were studied via solid-state NMR. A gold(III) cyanide, $K[Au(CN)_4]$, was also investigated. Carbon-13 and nitrogen-15 chemical shift tensors are reported for each salt, as are the measured ^{13}C,^{15}N direct dipolar coupling constants together with the related derived cyanide bond lengths, r(C,N). The value for r(C,N) in $[(n\text{-}C_4H_9)_4N][Au(CN)_2]$, 1.17(5) Å, was determined to be more realistic than a previously reported X-ray diffraction value of 1.03(4) Å. Large ^{13}C NMR line widths from $Tl[Au(CN)_2]$, 250−315 Hz, are attributed to coupling with ^{197}Au ($I = 3/2$) and/or $^{203/205}Tl$ ($I = 1/2$), as confirmed by measurements of the transverse relaxation constant, T_2. Investigation of the carbon-13 chemical shifts for cyanide ligands bound to gold involved in a variety of metallophilic bonding environments demonstrates that the chemical shift is sensitive to metallophilic bonding. Differences in Au−Tl metallophilic bonding are shown to cause a difference in the isotropic carbon-13 chemical shift of up to 15.7 ppm, while differences in Au−Au aurophilic bonding are found to be responsible for a change of up to 5.9 ppm. The disordered polymeric material gold(I) monocyanide, AuCN, was also investigated using ^{13}C and ^{15}N SSNMR. Two-dimensional ^{13}C,^{13}C double-quantum dipolar-recoupling spectroscopy was used to probe connectivity in this material. The ^{13}C NMR site multiplicity in AuCN is explained on the basis of sensitivity of the carbon-13 chemical shift to aurophilic bonding of the directly bonded gold atom. This assignment allows estimation of the position of the linear $[-M-CN-]_\infty$ chain's position with respect to the neighboring polymer chain. For the samples studied, a range of 7 ± 2% to 25 ± 5% of the AuCN chains are found to be "slipped" instead of aligned with the neighboring chains at the metal position.

1. Introduction

Molecules containing gold have been recognized for some time as having the potential to form an "extra" bond between closed-shell gold cations, despite the expected Coulombic repulsion.[1−5] While this interaction between heavy, closed-shell atoms has been assigned a variety of labels, for convenience we here apply the terms aurophilic, to describe gold−gold interactions, and metallophilic, to describe the analogous heteronuclear bonds. Metallophilic interactions are now understood to occur through a relativistic strengthening of the van der Waals interaction, an increase which can be enough to rival the energy of a hydrogen bond.[6] Much of the current research on gold compounds focuses on using aurophilic bonds for controlling supramolecular structures,[5,7−9] or studying the unusual photophysics often associated with the presence of aurophilic bonds.[6,10−12] For example, recent studies have found that the photoluminesence

* To whom correspondence should be addressed. Phone: (780)492-4336. Fax: (780)492-8231. E-mail: Roderick.Wasylishen@ualberta.ca.

(1) Jones, P G. *Gold Bull.* **1981**, *14*, 102–118.
(2) Jones, P. G. *Gold Bull.* **1983**, *16*, 114–124.
(3) Jones, P. G. *Gold Bull.* **1986**, *19*, 46–56.
(4) Scherbaum, F.; Grohmann, A.; Huber, B.; Krüger, C.; Schmidbaur, H. *Angew. Chem., Int. Ed.* **1988**, *27*, 1544–1546.
(5) Schmidbaur, H. *Chem. Soc. Rev.* **1995**, *24*, 391–400.
(6) Pyykkö, P. *Chem. Rev.* **1997**, *97*, 597–636.
(7) Braga, D.; Grepioni, F.; Desiraju, G. R. *Chem. Rev.* **1998**, *98*, 1375–1405.
(8) Leznoff, D. B.; Lefebvre, J. *Gold Bull.* **2005**, *38*, 47–54.
(9) Katz, M. J.; Sakai, K.; Leznoff, D. B. *Chem. Soc. Rev.* **2008**, *37*, 1884–1895.
(10) Gade, L. H. *Angew. Chem., Int. Ed.* **1997**, *36*, 1171–1173.
(11) Yam, V. W.-W.; Lo, K. K.-W. *Chem. Soc. Rev.* **1999**, *28*, 323–334.
(12) Yam, V. W.-W.; Cheng, E. C.-C. *Top. Curr. Chem.* **2007**, *281*, 269–309.

10.1021/ic8022198 CCC: $40.75 © 2009 American Chemical Society
Published on Web 01/23/2009

of gold-containing materials is influenced by factors such as temperature alteration,[13] freezing of a solution containing a gold(I) complex,[14] or introduction of an organic solvent to a solid gold(I) material, either as a vapor[15−19] or as a liquid.[20] Rational design of functional materials based on these properties is already underway in several labs: detection of alkali metal cations has been shown to be possible through the design of a suitable gold(I) compound with crown ether pendants,[21,22] and a sensor for volatile organic compounds based on the vapochromism of a gold(I) material has already been built.[15]

The cyano complexes of gold are of great commercial importance, through their useage in gold extraction,[23] and are also of medicinal interest.[24] Aurophilic interactions between gold atoms in approximately linear dicyanoaurate anions, $[NCAuCN]^-$, are strong enough that the anions associate into oligomers in solution[25,26] and also affect the structure of materials containing this anion.[5,7−9] Combining the abilities of both cyanide ligands and gold atoms to bridge metals, through bidentate or metallophilic bonding, has led to the development of new heterometallic network materials, with a plethora of novel features. Research into coordination polymers composed of cyanide and gold has been recently reviewed[8,9] and has continued to be an area of active research.[13,27−37] Coordination polymers of this type have demonstrated unusually high optical birefringence;[38,39] tunable electron lone-pair stereochemistry of Pb(II);[37] and the ability to reversibly absorb water,[40,41] organic vapors,[18] or ammonia,[19] the latter two causing an observable difference in the photophysics. The heterometallic nature of these polymers has also allowed the incorporation of metals with accessible high-spin electronic states, providing a means to study magnetic properties.[18,28,29,31,32,34−36,40−59] Magnetic exchange between electron spins on adjacent metal centers has been shown to occur along diamagnetic gold(I) or gold(III) cyanide chains.[18,35,40,43,45,54,57,58] As well, materials containing dicyanoaurate bridges and aurophilic bonds have been investigated in regard to promising behaviors with respect to transitions between high- and low-spin states of neighboring metals.[47,53]

(13) Assefa, Z.; Omary, M. A.; McBurnett, B. G.; Mohamed, A. A.; Patterson, H. H.; Staples, R. J.; Fackler, J. P., Jr. *Inorg. Chem.* **2002**, *41*, 6274–6280.
(14) White-Morris, R. L.; Olmstead, M. M.; Jiang, F.; Tinti, D. S.; Balch, A. L. *J. Am. Chem. Soc.* **2002**, *124*, 2327–2336.
(15) Bariáin, C.; Matías, I. R.; Romeo, I.; Garrido, J.; Laguna, M. *Appl. Phys. Lett.* **2000**, *77*, 2274–2276.
(16) Rawashdeh-Omary, M. A.; Omary, M. A.; Fackler, J. P., Jr.; Galassi, R.; Pietroni, B. R.; Burini, A. *J. Am. Chem. Soc.* **2001**, *123*, 9689–9691.
(17) Fernández, E. J.; López-de-Luzuriaga, J. M.; Monge, M.; Olmos, M. E.; Pérez, J.; Laguna, A.; Mohamed, A. A.; Fackler, J. P., Jr. *J. Am. Chem. Soc.* **2003**, *125*, 2022–2023.
(18) Lefebvre, J.; Batchelor, R. J.; Leznoff, D. B. *J. Am. Chem. Soc.* **2004**, *126*, 16117–16125.
(19) Katz, M. J.; Ramnial, T.; Yu, H.-Z.; Leznoff, D. B. *J. Am. Chem. Soc.* **2008**, *130*, 10662–10673.
(20) Vickery, J. C.; Olmstead, M. M.; Fung, E. Y.; Balch, A. L. *Angew. Chem., Int. Ed.* **1997**, *36*, 1179–1181.
(21) Yam, V. W.-W.; Li, C.-K.; Chan, C.-L. *Angew. Chem., Int. Ed.* **1998**, *37*, 2857–2859.
(22) Li, C.-K.; Lu, X.-X.; Wong, K. M.-C.; Chan, C.-L.; Zhu, N.; Yam, V. W.-W. *Inorg. Chem.* **2004**, *43*, 7421–7430.
(23) La Brooy, S. R.; Linge, H. G.; Walker, G. S. *Miner. Eng.* **1994**, *7*, 1213–1241.
(24) Ahmad, S. *Coord. Chem. Rev.* **2004**, *248*, 231–243.
(25) Rawashdeh-Omary, M. A.; Omary, M. A.; Patterson, H. H. *J. Am. Chem. Soc.* **2000**, *122*, 10371–10380.
(26) Rawashdeh-Omary, M. A.; Omary, M. A.; Patterson, H. H.; Fackler, J. P., Jr. *J. Am. Chem. Soc.* **2001**, *123*, 11237–11247.
(27) Che, C.-M.; Wong, W.-T.; Lai, T.-F.; Kwong, H.-L. *J. Chem. Soc., Chem. Commun.* **1989**, 243–244.
(28) Dong, W.; Sun, Y.-Q.; Yu, B.; Zhou, H.-B.; Song, H.-B.; Liu, Z.-Q.; Wang, Q.-M.; Liao, D.-Z.; Jiang, Z.-H.; Yan, S.-P.; Cheng, P. *New J. Chem.* **2004**, *28*, 1347–1351.
(29) Paraschiv, C.; Andruh, M.; Ferlay, S.; Hosseini, M. W.; Kyritsakas, N.; Planeix, J.-M.; Stanica, N. *Dalton Trans.* **2005**, 1195–1202.
(30) Siemeling, U.; Rother, D.; Bruhn, C.; Fink, H.; Weidner, T.; Träger, F.; Rothenberger, A.; Fenske, D.; Priebe, A.; Maurer, J.; Winter, R. *J. Am. Chem. Soc.* **2005**, *127*, 1102–1103.
(31) Xu, G.-F.; Liu, Z.-Q.; Zhou, H.-B.; Guo, Y.; Liao, D.-Z. *Aust. J. Chem.* **2006**, *59*, 640–646.
(32) Zhou, H.-B.; Wang, S.-P.; Liu, Z.-Q.; Liao, D.-Z.; Jiang, Z.-H.; Yan, S.-P.; Cheng, P. *Inorg. Chim. Acta* **2006**, *359*, 533–540.
(33) Chen, J.-X.; Zhang, W.-H.; Tang, X.-Y.; Ren, Z.-G.; Li, H.-X.; Zhang, Y.; Lang, J.-P. *Inorg. Chem.* **2006**, *45*, 7671–7680.
(34) Madalan, A. M.; Avarvari, N.; Andruh, M. *Cryst. Growth Des.* **2006**, *6*, 1671–1675.
(35) Katz, M. J.; Shorrock, C. J.; Batchelor, R. J.; Leznoff, D. B. *Inorg. Chem.* **2006**, *45*, 1757–1765.
(36) Qu, J.; Gu, W.; Liu, X. *J. Coord. Chem.* **2008**, *61*, 618–626.
(37) Katz, M. J.; Michaelis, V. K.; Aguiar, P. M.; Yson, R.; Lu, H.; Kaluarachchi, H.; Batchelor, R. J.; Schreckenbach, G.; Kroeker, S.; Patterson, H. H.; Leznoff, D. B. *Inorg. Chem.* **2008**, *47*, 6353–6363.
(38) Katz, M. J.; Aguiar, P. M.; Batchelor, R. J.; Bokov, A. A.; Ye, Z.-G.; Kroeker, S.; Leznoff, D. B. *J. Am. Chem. Soc.* **2006**, *128*, 3669–3676.
(39) Katz, M. J.; Kaluarachchi, H.; Batchelor, R. J.; Bokov, A. A.; Ye, Z.-G.; Leznoff, D. B. *Angew. Chem., Int. Ed.* **2007**, *46*, 8804–8807.
(40) Dong, W.; Zhu, L.-N.; Sun, Y.-Q.; Liang, M.; Liu, Z.-Q.; Liao, D.-Z.; Jiang, Z.-H.; Yan, S.-P.; Cheng, P. *Chem. Commun.* **2003**, 2544–2545.
(41) Colacio, E.; Lloret, F.; Kivekäs, R.; Ruiz, J.; Suárez-Varela, J.; Sundberg, M. R. *Chem. Commun.* **2002**, 592–593.
(42) Chu, I. K.; Shek, I. P. Y.; Siu, K. W. M.; Wong, W.-T.; Zuo, J.-L.; Lau, T.-C. *New J. Chem.* **2000**, *24*, 765–769.
(43) Leznoff, D. B.; Xue, B.-Y.; Patrick, B. O.; Sanchez, V.; Thompson, R. C. *Chem. Commun.* **2001**, 259–260.
(44) Leznoff, D. B.; Xue, B.-Y.; Stevens, C. L.; Storr, A.; Thompson, R. C.; Patrick, B. O. *Polyhedron* **2001**, *20*, 1247–1254.
(45) Leznoff, D. B.; Xue, B.-Y.; Batchelor, R. J.; Einstein, F. W. B.; Patrick, B. O. *Inorg. Chem.* **2001**, *40*, 6026–6034.
(46) Shorrock, C. J.; Xue, B.-Y.; Kim, P. B.; Batchelor, R. J.; Patrick, B. O.; Leznoff, D. B. *Inorg. Chem.* **2002**, *41*, 6743–6753.
(47) Niel, V.; Thompson, A. L.; Muñoz, M. C.; Galet, A.; Goeta, A. E.; Real, J. A. *Angew. Chem., Int. Ed.* **2003**, *42*, 3760–3763.
(48) Colacio, E.; Lloret, F.; Kivekäs, R.; Suárez-Varela, J.; Sundberg, M. R.; Uggla, R. *Inorg. Chem.* **2003**, *42*, 560–565.
(49) Shorrock, C. J.; Jong, H.; Batchelor, R. J.; Leznoff, D. B. *Inorg. Chem.* **2003**, *42*, 3917–3924.
(50) Stender, M.; White-Morris, R. L.; Olmstead, M. M.; Balch, A. L. *Inorg. Chem.* **2003**, *42*, 4504–4506.
(51) Vitoria, P.; Muga, I.; Gutiérrez-Zorrilla, J. M.; Luque, A.; Román, P.; Lezama, L.; Zúniga, F. J.; Beitia, J. I. *Inorg. Chem.* **2003**, *42*, 960–969.
(52) Zhou, H.-B.; Wang, S.-P.; Dong, W.; Liu, Z.-Q.; Wang, Q.-L.; Liao, D.-Z.; Jiang, Z.-H.; Yan, S.-P.; Cheng, P. *Inorg. Chem.* **2004**, *43*, 4552–4554.
(53) Galet, A.; Muñoz, M. C.; Martínez, V.; Real, J. A. *Chem. Commun.* **2004**, 2268–2269.
(54) Leznoff, D. B.; Shorrock, C. J.; Batchelor, R. J. *Gold Bull.* **2007**, *40*, 36–39.
(55) Lefebvre, J.; Callaghan, F.; Katz, M. J.; Sonier, J. E.; Leznoff, D. B. *Chem.—Eur. J.* **2006**, *12*, 6748–6761.
(56) Geisheimer, A. R.; Katz, M. J.; Batchelor, R. J.; Leznoff, D. B. *CrystEngComm* **2007**, *9*, 1078–1083.
(57) Katz, M. J.; Kaluarachchi, H.; Batchelor, R. J.; Schatte, G.; Leznoff, D. B. *Cryst. Growth Des.* **2007**, *7*, 1946–1948.
(58) Lefebvre, J.; Chartrand, D.; Leznoff, D. B. *Polyhedron* **2007**, *26*, 2189–2199.
(59) Lefebvre, J.; Trudel, S.; Hill, R. H.; Leznoff, D. B. *Chem.—Eur. J.* **2008**, *14*, 7156–7167.

Presented in the following is a ^{13}C and ^{15}N solid-state NMR, SSNMR, study of some prototype gold cyano complexes, in an effort to both investigate the interesting fundamental physics of these systems as well as to provide benchmark data and techniques useful for investigation of the cyanoaurate coordination polymers mentioned above. SSNMR studies of cyano ^{13}C and ^{15}N nuclei are well-known to provide useful information on cyanide-containing materials.[60−74] To date, ^{13}C and ^{15}N NMR parameters have only been reported for one cyano gold complex, Pb[Au(CN)$_2$](H$_2$O)$_x$ ($x = 0, 1$),[38] in the solid state. One aim of the present research is to determine the effect of structural changes, including changes in metallophilic bonding, on the NMR properties of the cyanide ligand. Samples investigated include the dicyanoaurate anion complexed with a series of counterions, $M^+[Au(CN)_2]^-$, where $M^+ = n$-butylammonium (no aurophilic interactions between anions),[75] potassium (anions associated via aurophilic bonds),[76] and thallium (both Au−Au and Au−Tl metallophilic bonding present).[77] In addition to data on these gold(I) dicyanides, we also present data for potassium tetracyanoaurate(III), in an effort to determine the effect of gold's formal oxidation state on the cyanide ligand NMR properties. NMR spectra of samples undergoing magic angle spinning (MAS) as well as stationary samples (where possible) were recorded to determine the ^{13}C and ^{15}N chemical shift tensors and ^{13}C,^{15}N dipolar coupling constants.

A SSNMR study of gold monocyanide, a material likely to possess as-yet unquantified modes of disorder, is also presented. Additionally, this study of AuCN provides an example of the information that can be determined using SSNMR to investigate a cyano gold coordination polymer. The monocyanides of the group 11 transition metals resisted structural characterization until recently, mainly due to disorder and poor sample crystallinity. A consistent picture of the structures of these materials has recently been built up from a combination of diffraction[78−85] and SSNMR/NQR[86,87] experiments. Two polymorphs of CuCN are known, and structures of both the high-temperature, HT-CuCN, and low-temperature, LT-CuCN, polymorphs of CuCN have been determined.[79,80,83−85] In HT-CuCN, AgCN, and AuCN, the materials are composed of infinite, linear $[-M-CN-]_\infty$ chains,[79,81,82] with neighboring chains aligned at the metal for AuCN, but staggered for HT-CuCN and AgCN. Chain alignment in AuCN presumably arises from the favorable energetics of forming aurophilic bonds.[78] LT-CuCN is also comprised of infinite MCN chains, but these are packed together in a more complicated way, with bond angles along the chain deviating slightly from 180°, ranging from 174.0 to 179.3°.[80] Interestingly, neighboring MCN chains in LT-CuCN are also lined up at the metal, for example, in two neighboring chains, d(Cu3−Cu3) = 2.997 Å. In the group 11 monocyanides, it is not possible to differentiate the carbon from the nitrogen atoms using diffraction experiments, making the orientation of the cyanide ligands in these chains unknown.[78−85] The relative orientation of cyanide ligands on opposing sides of the metal in CuCN and AgCN has been investigated using SSNMR and NQR spectroscopy.[86,87] In these studies, it was determined that there is significant "head−tail" disorder of the cyanide ligands. In both materials, 30 ± 10% of the metal sites have the two coordinating cyanides in opposite orientation, [−NC−Ag−CN−] or [−CN−Ag−NC−], while 70 ± 10% have the two cyanides in the same orientation, [−CN−Ag−CN−].[86,87] Diffraction studies have shown that another type of disorder in these materials is also likely: static disorder of the long chains with respect to each other.[79,81,82] Presented below is a ^{13}C and ^{15}N SSNMR study of AuCN to investigate the possibility of cyanide orientational disorder, and to probe for the presence of stacking faults in the chain alignments.

(60) Avalle, P.; Harris, R. K.; Hanika-Heidl, H.; Fischer, R. D. *Solid State Sci.* **2004**, *6*, 1069–1076.
(61) Poll, E.-M.; Schütze, J.-U.; Fischer, R. D.; Davies, N. A.; Apperley, D. C.; Harris, R. K. *J. Organomet. Chem.* **2001**, *621*, 254–260.
(62) Poll, E.-M.; Olbrich, F.; Samba, S.; Fischer, R. D.; Avalle, P.; Apperley, D. C.; Harris, R. K. *J. Solid State Chem.* **2001**, *157*, 324–338.
(63) Poll, E.-M.; Samba, S.; Fischer, R. D.; Olbrich, F.; Davies, N. A.; Avalle, P.; Apperley, D. C.; Harris, R. K. *J. Solid State Chem.* **2000**, *152*, 286–301.
(64) Siebel, E.; Fischer, R. D.; Davies, N. A.; Apperley, D. C.; Harris, R. K. *J. Organomet. Chem.* **2000**, *604*, 34–42.
(65) Bowmaker, G. A.; Churakov, A. V.; Harris, R. K.; Oh, S.-W. *J. Organomet. Chem.* **1998**, *550*, 89–99.
(66) Brimah, A. K.; Schwarz, P.; Fischer, R. D.; Davies, N. A.; Harris, R. K. *J. Organomet. Chem.* **1998**, *568*, 1–12.
(67) Schwarz, P.; Siebel, E.; Fischer, R. D.; Davies, N. A.; Apperley, D. C.; Harris, R. K. *Chem.—Eur. J.* **1998**, *4*, 919–926.
(68) Siebel, E.; Fischer, R. D.; Kopf, J.; Davies, N. A.; Apperley, D. C.; Harris, R. K. *Inorg. Chem. Commun.* **1998**, *1*, 346–349.
(69) Schütze, J.-U.; Eckhardt, R.; Fischer, R. D.; Apperley, D. C.; Davies, N. A.; Harris, R. K. *J. Organomet. Chem.* **1997**, *534*, 187–194.
(70) Davies, N. A.; Harris, R. K.; Olivieri, A. C. *Mol. Phys.* **1996**, *87*, 669–677.
(71) Eller, S.; Schwarz, P.; Brimah, A. K.; Fischer, R. D.; Apperley, D. C.; Davies, N. A.; Harris, R. K. *Organometallics* **1993**, *12*, 3232–3240.
(72) Behrens, U.; Brimah, A. K.; Soliman, T. M.; Fischer, R. D.; Apperley, D. C.; Davies, N. A.; Harris, R. K. *Organometallics* **1992**, *11*, 1718–1726.
(73) Apperley, D. C.; Davies, N. A.; Harris, R. K.; Brimah, A. K.; Eller, S.; Fischer, R. D. *Organometallics* **1990**, *9*, 2672–2676.
(74) Wu, G.; Wasylishen, R. E. *J. Phys. Chem.* **1993**, *97*, 7863–7869.
(75) Schubert, R. J.; Range, K.-J. *Z. Naturforsch., B: Chem. Sci.* **1990**, *45*, 1118–1122.
(76) Rosenzweig, A.; Cromer, D. T. *Acta Crystallogr.* **1959**, *12*, 709–712.
(77) Blom, N.; Ludi, A.; Bürgi, H.-B.; Tichý, K. *Acta Crystallogr., Sect. C* **1984**, *40*, 1767–1769.
(78) Bowmaker, G. A.; Kennedy, B. J.; Reid, J. C. *Inorg. Chem.* **1998**, *37*, 3968–3974.
(79) Hibble, S. J.; Cheyne, S. M.; Hannon, A. C.; Eversfield, S. G. *Inorg. Chem.* **2002**, *41*, 4990–4992.
(80) Hibble, S. J.; Eversfield, S. G.; Cowley, A. R.; Chippindale, A. M. *Angew. Chem., Int. Ed.* **2004**, *43*, 628–630.
(81) Hibble, S. J.; Cheyne, S. M.; Hannon, A. C.; Eversfield, S. G. *Inorg. Chem.* **2002**, *41*, 1042–1044.
(82) Hibble, S. J.; Hannon, A. C.; Cheyne, S. M. *Inorg. Chem.* **2003**, *42*, 4724–4730.
(83) Reckeweg, O.; Simon, A. *Z. Naturforsch., B: Chem. Sci.* **2002**, *57*, 895–900.
(84) Reckeweg, O.; Lind, C.; Simon, A.; DiSalvo, F. J. *Z. Naturforsch., B: Chem. Sci.* **2003**, *58*, 155–158.
(85) Wang, J.; Collins, M. F.; Johari, G. P. *Phys. Rev. B: Condens. Matter Mater. Phys.* **2002**, *65*, 180103.
(86) Kroeker, S.; Wasylishen, R. E.; Hanna, J. V. *J. Am. Chem. Soc.* **1999**, *121*, 1582–1590.
(87) Bryce, D. L.; Wasylishen, R. E. *Inorg. Chem.* **2002**, *41*, 4131–4138.

2. NMR Terminology and Theory

We summarize here the interactions that affect the carbon-13 and nitrogen-15 SSNMR spectra of these aurocyanide materials, along with the terminology and conventions used to describe them. Some background theory of the NMR experiments, as well as the information garnered from each will also be described. All of the studied samples made use of ^{13}C,^{15}N dilabeled cyanide ligands, and therefore the discussion that follows will focus on a heteronuclear pair of spin-1/2 nuclei. The possibility of coupling interactions with the relatively small magnetic moment of Au-197 ($I = 3/2$, natural abundance = 100%) is also discussed.

The observed chemical shift of a nucleus depends on the orientation of the externally applied magnetic field, B_0, with respect to the molecular features. This orientation dependence is represented by the second-rank chemical shift tensor,[88,89] or CS tensor, generally assumed to be a symmetric tensor.[89,90] When represented in its principal axis system, a symmetric tensor is diagonal and thus has only three elements. By convention, the values of these three elements for each CS tensor are labeled in decreasing order as $\delta_{11} \geq \delta_{22} \geq \delta_{33}$.[91] The chemical shift of a nucleus is thus fully described by δ_{11}, δ_{22}, and δ_{33} in combination with a specification of how the principal axis system is oriented in the molecule. For spectra of samples spinning rapidly at the 54.736° magic angle, the anisotropic chemical shift of a powder is averaged to δ_{iso}. If the spinning is at a rate comparable to the breadth of the magnetic shielding interaction in hertz, the broad static spectrum is replaced by a combination of spinning sidebands whose intensities encode the elements of the CS tensor.[92−94]

It is often convenient to describe the CS tensor using an alternate set of three elements: the isotropic or average shift, $\delta_{iso} = (\delta_{11} + \delta_{22} + \delta_{33})/3$, the span, $\Omega = \delta_{11} - \delta_{33}$, and the skew, $\kappa = 3(\delta_{iso} - \delta_{22})/\Omega$.[91] For any nucleus at a site with higher than 2-fold rotational symmetry, two of the principal components are equal to each other, that is, $\kappa = \pm 1$, and the CS tensor is axially symmetric.[89,95,96] It should be noted that the procedure of fitting sideband intensities has difficulty in differentiating axially symmetric CS tensors from those that deviate slightly from axial symmetry.[94,97]

Energy levels of a ^{13}C nucleus in a ^{13}C,^{15}N-labeled cyanide are perturbed by the magnetic field generated by the proximal ^{15}N nucleus (and vice versa). The familiar *J* coupling, passed on through the bond, is generally less than 20 Hz and thus too small to affect these spectra.[87,98−100] There is also a through-space interaction, or direct dipolar coupling, described by the constant R_{DD}:[101]

$$R_{DD} = \left(\frac{\mu_0 \hbar}{8\pi^2}\right)\gamma_I \gamma_S \langle r_{IS}^{-3} \rangle \quad (1)$$

where γ_I is the strength of the magnetic dipole moment of nucleus I, ^{13}C or ^{15}N here, and $\langle r_{IS}^{-3} \rangle$ is the averaged inverse cube of the distance between the two nuclei. The magnitude of this interaction is approximately 2 kHz for the ^{13}C,^{15}N spin pair in a cyanide ligand and depends strongly on the internuclear separation, thereby providing a direct measure of the C−N bond distance. It should be noted that a portion of the *J*-coupling tensor has the same geometrical dependence as the dipolar coupling interaction, and experiments actually measure a combination of these two effects, termed the effective dipolar coupling constant, R_{eff}.[101,102] As has been noted previously,[87] the difference between R_{eff} and R_{DD} is expected to be less than 20 Hz for a cyano ^{13}C,^{15}N spin pair. Since this is less than the experimental error associated with measuring R_{eff}, we have assumed $R_{DD} = R_{eff}$.

A distance measured via the NMR observable R_{eff} has a slightly different dependence on vibrational averaging than does an X-ray or neutron diffraction distance measurement, typically leading to a disagreement of a few percent. This difference in averaging is known to yield a 1−4% longer bond distance for C−C distances measured via NMR as compared to diffraction distance determinations.[103−105] In a study of AgCN, it was argued that a value for the C−N bond length more amenable to direct comparison with diffraction data could be produced by shortening the NMR-measured length by 2.5 ± 1.5%.[87] All distance measurements reported here include this vibrational correction of shortening the NMR-derived bond lengths and applying the concomitant increase in error ranges.

Spectra from a stationary sample of a ^{13}C,^{15}N-labeled cyanide, observing either ^{13}C or ^{15}N, manifest effects from the anisotropy of both the chemical shift and dipolar coupling to the neighboring spin-1/2 nucleus. Analysis of such spectra therefore allows one to obtain both interaction tensors as well as their relative orientations from the observed line

(88) Grant, D. M. Chemical Shift Tensors In *Encyclopedia of Nuclear Magnetic Resonance*; Grant, D. M., Harris, R. K., Eds.; John Wiley and Sons: Chichester, U.K., 1996; Vol. *2*, pp 1298.
(89) Anet, F. A. L.; O'Leary, D. J. *Concepts Magn. Res.* **1991**, *3*, 193–214.
(90) Schneider, R. F. *J. Chem. Phys.* **1968**, *48*, 4905–4909.
(91) Mason, J. *Solid State Nucl. Magn. Reson.* **1993**, *2*, 285–288.
(92) Maricq, M. M.; Waugh, J. S. *J. Chem. Phys.* **1979**, *70*, 3300–3316.
(93) Herzfeld, J.; Berger, A. E. *J. Chem. Phys.* **1980**, *73*, 6021–6030.
(94) Harris, R. K.; Olivieri, A. C. Spinning Sideband Analysis for Spin-1/2 Nuclei In *Encyclopedia of Nuclear Magnetic Resonance*; Grant, D. M., Harris, R. K., Eds.; John Wiley and Sons: Chichester, 2002; Vol. *9*, pp 141.
(95) Buckingham, A. D.; Malm, S. M. *Mol. Phys.* **1971**, *22*, 1127–1130.
(96) Robert, J. B.; Wiesenfeld, L. *Phys. Rep.* **1982**, *86*, 363–401.
(97) Clayden, N. J.; Dobson, C. M.; Lian, L.-Y.; Smith, D. J. *J. Magn. Reson.* **1986**, *69*, 476–487.
(98) Friesen, K. J.; Wasylishen, R. E. *J. Magn. Reson.* **1982**, *48*, 152–154.
(99) Eichele, K.; Wasylishen, R. E. *Solid State Nucl. Magn. Reson.* **1992**, *1*, 159–163.
(100) Barszczewicz, A.; Helgaker, T.; Jaszuński, M.; Jørgensen, P.; Ruud, K. *J. Magn. Reson., Ser. A* **1995**, *114*, 212–218.
(101) Wasylishen, R. E. Dipolar and Indirect Coupling Tensors in Solids In *Encyclopedia of Nuclear Magnetic Resonance*; Grant, D. M., Harris, R. K., Eds.; John Wiley and Sons: Chichester, U.K., 1996; Vol. *3*, pp 1685.
(102) Wasylishen, R. E. Indirect Nuclear Spin-Spin Coupling Tensors In *Encyclopedia of Nuclear Magnetic Resonance*; Grant, D. M., Harris, R. K., Eds.; John Wiley and Sons: Chichester, U.K., 2002; Vol. *9*, pp 274.
(103) Millar, J. M.; Thayer, A. M.; Zax, D. B.; Pines, A. *J. Am. Chem. Soc.* **1986**, *108*, 5113–5116.
(104) Nakai, T.; Ashida, J.; Terao, T. *Mol. Phys.* **1989**, *67*, 839–847.
(105) Ishii, Y.; Terao, T.; Hayashi, S. *J. Chem. Phys.* **1997**, *107*, 2760–2774.

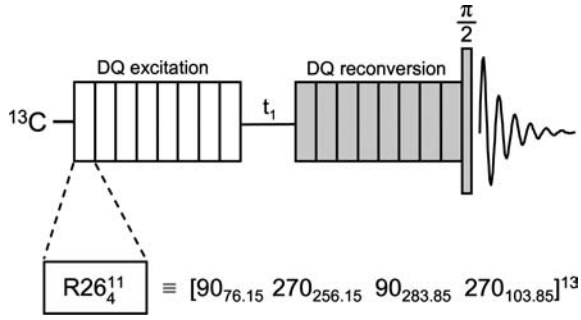

Figure 1. Symbolic display of the $SR26_4^{11}$ pulse sequence. Pulses in the $R26_4^{11}$ block are shown using the $(\text{Pulse Angle})_{\text{Phase}}$ convention.

shape.[106−109] This relative orientation is given here using the angle β to define the angle between $r_{(C,N)}$ and δ_{33}, while α is used to define the angle between δ_{11} and the projection of $r_{(C,N)}$ in the δ_{11},δ_{22} plane. In many cyanides, ^{13}C and ^{15}N CS tensors have δ_{33} along the CN bond, in which case the value of β is zero, and α may be taken as zero as well (when $\beta = 0°$, $r_{(C,N)}$ is coincident with δ_{33} and creates no projection on the δ_{11},δ_{22} plane, making α unnecessary). In spectra of AX spin systems spun at the magic angle at a rate less than Ω in frequency units, spinning sidebands are generated, whose intensities are modulated both by the chemical shift tensor and the dipolar coupling to the neighboring spin-1/2 nucleus.[94] Spectral simulations therefore require inclusion of both interactions, and we applied the program SPINEVOLUTION to determine CS tensor elements.[110]

There is a library of techniques available which make use of the resolution afforded by MAS but retains information from homonuclear dipolar couplings.[111,112] We applied the supercycled $SR26_4^{11}$ sequence, which has been tailored, using symmetry principles,[113] for the combination of a small R_{eff} and a large Ω required to recouple intermolecular ^{13}C cyanide sites.[114,115] In the present study, we use this dipolar-recoupling pulse sequence to investigate proximity, that is, to determine whether pairs of peaks arise from sites within the same material. A one-channel, two-dimensional version of this pulse sequence, see Figure 1, was applied.[116,117] The first half of the sequence excites a double-quantum coherence using a long train of composite 180° pulses, which is then allowed to evolve in the indirect dimension for a time t_1, before being converted back to longitudinal magnetization by the second block of composite 180° pulses, which is finally observed using a $\pi/2$ read pulse.

In each compound, the carbon, and in AuCN, the nitrogen, atoms are directly bonded to gold, internuclear coupling with which can affect the spin-1/2 NMR spectra. Gold-197 is a quadrupolar nucleus with a small magnetic moment (<1/50th that of ^1H) and a large nuclear quadrupole moment ($Q = 54.7$ fm^2).[118] The ^{197}Au nucleus may perturb the energy levels of neighboring ^{13}C or ^{15}N nuclei through both spin−spin coupling pathways described above: J coupling and direct dipolar coupling. As mentioned above, the direct dipolar coupling between two spin-1/2 nuclei is averaged to zero when the sample is spun rapidly at the magic angle. For a spin-1/2 nucleus coupled to a nucleus with a large quadrupolar coupling constant, however, the direct dipolar coupling between the two cannot be averaged to zero by magic-angle spinning, and a residual dipolar coupling remains.[119] For many systems studied at room temperature, ^{197}Au relaxes so rapidly that no effects on the spin-1/2 NMR spectra are observed; however, there have been examples in which spin−spin coupling to ^{197}Au has been observed in ^{31}P NMR spectra.[120−126]

As an example of the effects expected from residual dipolar coupling to ^{197}Au, we here estimate the ^{13}C line shape of $K[Au(CN)_2]$ expected from such an interaction. In this approximately linear molecule, the ^{197}Au EFG tensor is likely axially symmetric with V_{zz} along the Au−C bond. An approximate value of $C_Q(^{197}Au)$, 1.27 GHz, has been obtained from Mössbauer data for $K[Au(CN)_2]$ at 4.2 K.[127] However, because of the low Larmor frequency of ^{197}Au, the simulated spectra are nearly invariant to the magnitude of C_Q as long as it is greater than ~300 MHz. With the orientation and principal components of the EFG tensor so defined, spectral simulations of the line shape need include only two variables: R_{eff} and J_{iso}.[119] The published crystal structure allows an initial estimate of 69 Hz for R_{eff} to be set from the Au−C bond length. An estimate of the expected $J_{\text{iso}}(^{197}Au,^{13}C)$ can be determined through comparison to an analogous system,

(106) VanderHart, D. L.; Gutowsky, H. S. *J. Chem. Phys.* **1968**, *49*, 261–271.
(107) Zilm, K. W.; Grant, D. M. *J. Am. Chem. Soc.* **1981**, *103*, 2913–2922.
(108) Power, W. P.; Wasylishen, R. E. *Annu. Rep. NMR Spectrosc.* **1991**, *23*, 1–84.
(109) Eichele, K.; Wasylishen, R. E. *J. Magn. Reson., Ser. A* **1994**, *106*, 46–56.
(110) Veshtort, M.; Griffin, R. G. *J. Magn. Reson.* **2006**, *178*, 248–282.
(111) Schnell, I. *Prog. Nucl. Magn. Reson. Spectrosc.* **2004**, *45*, 145–207.
(112) Griffiths, J. M.; Bennett, A. E.; Griffin, R. G. Homonuclear Recoupling Schemes in MAS NMR In *Encyclopedia of Nuclear Magnetic Resonance*; Grant, D. M., Harris, R. K., Eds.; John Wiley and Sons: Chichester, U.K., 1996; Vol. *4*, pp 2390.
(113) Levitt, M. H. Symmetry-Based Pulse Sequences in Magic-Angle Spinning Solid-State NMR In *Encyclopedia of Nuclear Magnetic Resonance*; Grant, D. M., Harris, R. K., Eds.; John Wiley and Sons: Chichester, U.K., 2002; Vol. *9*, pp 165.
(114) Kristiansen, P. E.; Carravetta, M.; Lai, W. C.; Levitt, M. H. *Chem. Phys. Lett.* **2004**, *390*, 1–7.
(115) Kristiansen, P. E.; Carravetta, M.; van Beek, J. D.; Lai, W. C.; Levitt, M. H. *J. Chem. Phys.* **2006**, *124*, 234510.
(116) Brouwer, D. H.; Kristiansen, P. E.; Fyfe, C. A.; Levitt, M. H. *J. Am. Chem. Soc.* **2005**, *127*, 542–543.
(117) Brouwer, D. H.; Darton, R. J.; Morris, R. E.; Levitt, M. H. *J. Am. Chem. Soc.* **2005**, *127*, 10365–10370.
(118) Harris, R. K.; Becker, E. D.; Cabral de Menezes, S. M.; Goodfellow, R.; Granger, P. *Pure Appl. Chem.* **2001**, *73*, 1795–1818.
(119) Olivieri, A. *Solid State Nucl. Magn. Reson.* **1992**, *1*, 345–353.
(120) Barron, P. F.; Engelhardt, L. M.; Healy, P. C.; Oddy, J.; White, A. H. *Aust. J. Chem.* **1987**, *40*, 1545–1555.
(121) Attar, S.; Bearden, W. H.; Alcock, N. W.; Alyea, E. C.; Nelson, J. H. *Inorg. Chem.* **1990**, *29*, 425–433.
(122) Berners-Price, S. J.; Colquhoun, L. A.; Healy, P. C.; Byriel, K. A.; Hanna, J. V. *J. Chem. Soc., Dalton Trans.* **1992**, 3357–3363.
(123) Baker, L.-J.; Bowmaker, G. A.; Healy, P. C.; Skelton, B. W.; White, A. H. *J. Chem. Soc., Dalton Trans.* **1992**, 989–997.
(124) Angermair, K.; Bowmaker, G. A.; de Silva, E. N.; Healy, P. C.; Jones, B. E.; Schmidbaur, H. *J. Chem. Soc., Dalton Trans.* **1996**, 3121–3129.
(125) de Silva, E. N.; Bowmaker, G. A.; Healy, P. C. *J. Mol. Struct.* **2000**, *516*, 263–272.
(126) Healy, P. C.; Loughrey, B. T.; Bowmaker, G. A.; Hanna, J. V. *Dalton Trans.* **2008**, 3723–3728.
(127) Faltens, M. O.; Shirley, D. A. *J. Chem. Phys.* **1970**, *53*, 4249–4264.

using the reduced coupling constant,[102,128] $K(I,S)=4\pi^2h^{-1}[J(I,S)/\gamma_I\gamma_S]$. Analogous molecules where one nucleus is replaced by a heavier congener are typified by a larger K because of increased electron density at the nucleus. For example, in the analogous series of linear $ClM(PR_3)$ (where M = Cu, Ag, Au), $^1K_{iso}$(M,P) approximately doubles for each step down the periodic table.[123] Also, the value of $^1K_{iso}$(M,C) in AgCN is approximately double that of CuCN. This same numerical relationship between J couplings in analogous molecules does not hold across the entire periodic table but seems to be useful within the group 11 metals. The values of $^1K_{iso}$(Au,C) in $[Au(CN)_2]^-$ anions are therefore likely close to double the value of $^1K_{iso}$(Ag,C) in ···CNAgCNAgCN···, and a value of $J_{iso}(^{197}Au,^{13}C) \simeq 180$ Hz is predicted. Lineshape simulations, using WSOLIDS,[129] show that the expected spectrum is composed of four peaks separated by 60 to 160 Hz, covering a total range of ~400 Hz. Even if the J coupling is 0, R_{eff} alone is enough to cause the four peaks of the simulated spectrum to cover a range of ~250 Hz. We therefore expect that residual dipolar coupling to ^{197}Au will have a noticeable effect on the ^{13}C spectra, unless the gold nucleus is self-decoupled by rapid relaxation.

3. Experimental Section

3.1. Sample Preparation. A sample of AuCN used as starting material was prepared from commercial $K[Au(CN)_2]$ through treatment with HCl according to literature methods.[130] The sample of ^{13}C,^{15}N-labeled $K[Au(CN)_2]$ was prepared via dissolution of AuCN in a hot aqueous solution of 99% ^{13}C,^{15}N-labeled KCN, followed by recrystallization from hot water.[130] The ^{13}C,^{15}N-labeled $[(n\text{-}C_4H_9)_4N][Au(CN)_2]$ was prepared by dissolution of AuCN in a hot aqueous solution of 60% ^{13}C,^{15}N-labeled KCN, followed by precipitation with an aqueous solution of tetra-*n*-butylammonium chloride, and then recrystallization from hot water.[75] We found it necessary to spin the sample at less than ~6 kHz during MAS experiments to prevent the sample of $[(n\text{-}C_4H_9)_4N][Au(CN)_2]$ from melting. The sample of ^{13}C,^{15}N-labeled $Tl[Au(CN)_2]$ was prepared by dissolution of AuCN in a hot aqueous solution of 60% ^{13}C,^{15}N-labeled KCN, followed by precipitation with an aqueous solution of Tl_2SO_4 and recrystallization from hot water.[77] A sample of $K[AuBr_2(CN)_2]$ for use as a starting material was prepared by the oxidation of commercial $K[Au(CN)_2]$ with a solution of Br_2 in MeOH followed by recrystallization from hot water.[131] This material was then added to a methanol solution of 99% ^{13}C,^{15}N-labeled KCN, and the result recrystallized from hot water to yield $K[Au(CN)_4]$, which was then dehydrated under a high vacuum at room temperature.[131] The identities of $K[Au(CN)_2]$, $Tl[Au(CN)_2]$, and $[(n\text{-}C_4H_9)_4N][Au(CN)_2]$ were confirmed by matching the experimental and theoretical X-ray powder diffraction patterns.[75−77] Only the hydrate of $K[Au(CN)_4]$ has a known crystal structure, but this material was found to dehydrate too rapidly for identification by powder XRD. Therefore, the identity of $K[Au(CN)_4]$ was confirmed by matching the 2189.5 cm^{-1} CN stretch to the published 2189 cm^{-1} value,[131] and the fact that only a single ^{13}C NMR peak is observed in the solid state.

Gold monocyanide was prepared via three synthetic routes. AuCN(A) was synthesized using the method given in U.S Patent #4,222,996.[132] Metallic gold was dissolved in aqua regia, diluted with distilled water, and treated with aqueous KOH to a pH of ~12, then reduced with 0.75 equiv of Na_2SO_3, followed by treatment with 50% ^{13}C,^{15}N-labeled KCN and acidification with HCl to a pH of ~2. It was found that complete removal of the starting materials required soaking this material in distilled water for 1 week at room temperature. This wash water was then removed by filtration, washing with several volumes of water, and finally with MeOH. A second preparation of AuCN was also performed, with all details the same as in AuCN(A), except for the use of a 10% excess of the reducing agent, Na_2SO_3. This method produced AuCN(A′), a material with a greenish color instead of the reported yellow of AuCN. A third synthetic method produced yellow-colored AuCN(B) from 50% ^{13}C,^{15}N-labeled $K[Au(CN)_2]$, prepared as described above, by treatment with HCl at 60−70 °C.[130] Characterization of these materials by SSNMR, IR, and X-ray diffraction is discussed below.

Powder XRD measurements used an Inel powder diffractometer with copper $K\alpha_1$ radiation. IR spectra were collected on a Nic-Plan FTIR Microscope, including a reinvestigation of AgCN samples discussed in a previous publication.[87,156]

3.2. SSNMR. Carbon-13 NMR spectra were acquired at 50.3 MHz (4.70 T) using a Chemagnetics CMX Infinity 200, at 75.5 MHz (7.05 T) using a Bruker Avance 300, or at 125.8 MHz (11.75 T) with a Bruker Avance 500. All ^{13}C experiments used powdered samples packed in 4-mm-outer-diameter rotors, were recorded using 4 μs $\pi/2$ pulses, and were referenced to TMS by setting the high-frequency peak of an external adamantane sample to 38.56 ppm.[133] For all samples except $[(n\text{-}C_4H_9)_4N][Au(CN)_2]$, Bloch-decay experiments were used for MAS spectra, while Hahn-echo experiments were used for spectra of stationary samples. Experiments used pulse delays of 25 min for $K[Au(CN)_2]$, 30 min for $Tl[Au(CN)_2]$, 30 min (but using a 45° pulse) for $K[Au(CN)_4]$, and 20 min for AuCN. Variable-amplitude[134] cross polarization[135−137] from the protons in the tetra-*n*-butylammonium cation was used to collect ^{13}C NMR spectra of $[(n\text{-}C_4H_9)_4N][Au(CN)_2]$, under the Hartmann−Hahn match condition, and TPPM decoupling[138] at a power level of ~60 kHz was applied during acquisition. Under these conditions, a 10 s pulse delay was utilized for both the CPMAS and static CP Hahn-echo experiments.

Two-dimensional ^{13}C homonuclear dipolar-recoupling experiments used the $SR26_4^{11}$ pulse sequence.[114−117] Phase cycling and pulse timings were those of the published sequence.[117] Pure absorption spectra were obtained using the States method, and recoupling-field power levels were experimentally optimized. The pulse sequence was benchmarked using 60% 1-^{13}C-labeled glycine, Raylo Chemicals, in which intermolecular distances are short enough to allow ^{13}C,^{13}C recoupling.[115] Setup spectra of 60% 1-^{13}C-labeled glycine were obtained at a MAS rate of 8.097 kHz, using two excitation blocks totaling 3.95 ms; DQ recoupling efficiencies

(128) Jameson, C. J. Spin-Spin Coupling In *Multinuclear NMR*; Mason, J., Ed.; Plenum Press: New York, 1987; pp 89.
(129) Eichele, K.; Wasylishen, R. E. *WSOLIDS*, version 2.0.18; University of Alberta: Edmonton, Canada, 2000.
(130) Bradley, R. S.; Munro, D. C.; Spencer, P. N. *Trans. Faraday Soc.* **1969**, *65*, 1920–1926.
(131) Jones, L. H.; Smith, J. M. *J. Chem. Phys.* **1964**, *41*, 2507–2511.
(132) Okinaka, Y.; Smith, L. E. U.S. Patent 4,222,996, 1980.
(133) Earl, W. L.; VanderHart, D. L. *J. Magn. Reson.* **1982**, *48*, 35–54.
(134) Peersen, O. B.; Wu, X.; Kustanovich, I.; Smith, S. O. *J. Magn. Reson., Ser. A* **1993**, *104*, 334–339.
(135) Hartmann, S. R.; Hahn, E. L. *Phys. Rev.* **1962**, *128*, 2042–2053.
(136) Pines, A.; Gibby, M. G.; Waugh, J. S. *J. Chem. Phys.* **1972**, *56*, 1776–1777.
(137) Pines, A.; Gibby, M. G.; Waugh, J. S. *J. Chem. Phys.* **1973**, *59*, 569–590.
(138) Bennett, A. E.; Rienstra, C. M.; Auger, M.; Lakshmi, K. V.; Griffin, R. G. *J. Chem. Phys.* **1995**, *103*, 6951–6958.

Table 1. Local Structural Parameters for Gold(I) Cyanides

salt	Au site	C−N bond (Å)	Au−C bond (Å)	C−Au−C angle (deg.)	Au−C−N angle (deg.)	Au−Au (Å)	Au−Tl (Å)
$K[Au(CN)_2]$[a]		1.17(20)	2.12(14)	180	173(7.5)	4@3.64	
$[(n\text{-}C_4H_9)_4N][Au(CN)_2]$[b]		1.03(4)	1.96(4)	180	174(3)	4@8.05	
$Tl[Au(CN)_2]$[c]	1	1.148(2)	1.970(2)	180	180	2@3.560	
		1.148(2)	1.971(2)	180	180		
	2	1.145(2)	1.971(2)	180	180	2@3.560	
		1.146(2)	1.970(2)	180	180	2@3.037	
	3	1.145(2)	1.972(2)	180	176.6(4)	2@3.037	3.463
		1.148(2)	1.971(2)	177.1(2)	175.8(4)	2@3.068	3.446

[a] Data from the X-ray diffraction study of Rosenzweig and Cromer.[76] [b] Data from an X-ray diffraction study of Schubert and Range.[75] [c] Neutron diffraction study by Blom et al.[77]

similar to reported values were obtained.[114,115] Recoupling experiments performed on AuCN used a MAS rate of 9.615 kHz, and three $SR26_4^{11}$ DQ-excitation blocks totaling 4.992 ms.

Nitrogen-15 NMR spectra were collected at 20.3 MHz (4.70 T) using a Chemagnetics CMX Infinity 200, at 30.5 MHz (7.05 T) with a Bruker Avance 300, at 50.7 MHz (11.75 T) using a Bruker Avance 500, or at 91.2 MHz (21.14 T) using a Bruker Avance II 900. All experiments used 4 mm rotors, and peaks were referenced by setting the low-frequency peak of an external sample of ammonium nitrate to 23.8 ppm (with respect to neat liquid ammonia at 0 ppm).[139] The MAS spectra, except those of $[(n\text{-}C_4H_9)_4N][Au(CN)_2]$, used Bloch-decay experiments. Experiments used a B_1 field sufficient to generate a 5 μs $\pi/2$ pulse for experiments recorded at 4.70, 7.05, and 11.75 T, while a 9 μs $\pi/2$ pulse strength was applied for experiments at 21.14 T. Spectra of $K[Au(CN)_2]$ used a 30° excitation pulse and 40 min recycle delay. $Tl[Au(CN)_2]$ required a 10 min pulse delay when applying a 30° pulse. $K[Au(CN)_4]$ required a 30 min delay when using a 20° pulse, and AuCN samples used a 10 min delay and a 20° excitation pulse. Variable-amplitude[134] cross polarization[135−137] followed by TPPM decoupling[138] at a power level of ~60 kHz during acquisition was used for the ^{15}N MAS spectra of $[(n\text{-}C_4H_9)_4N][Au(CN)_2]$, and CP followed by a 180° refocusing pulse was used for static spectra.

Carbon-13 and nitrogen-15 NMR spectra from stationary samples were simulated using WSOLIDS,[129] while nitrogen-15 spectra from slow-spinning samples were simulated using SPINEVOLUTION.[110] Simulated ^{13}C spectra from MAS samples including residual dipolar coupling to ^{197}Au were calculated using WSOLIDS.[129] We found the programs SIMPSON[140] and SPINEVOLUTION[110] invaluable for theoretically comparing various recoupling conditions used in the $SR26_4^{11}$ pulse sequence.

4. Results and Discussion

4.1. ^{13}C NMR of Gold(I) Dicyanides. A sample of $K[Au(CN)_2]$ was prepared and investigated using ^{13}C SSNMR. The structure, reported in 1959 by Rosenzweig and Cromer,[76] contains alternating sheets of potassium and gold atoms with cyanide ligands above and below the gold plane. The local structure around the single unique CN moiety, reported in Table 1, has the unique Au atom surrounded by four Au neighbors at 3.64 Å, close enough for aurophilic bonding to be present.[141,142] Presented in Figure 2 is the ^{13}C NMR spectrum of a stationary sample of 50% ^{13}C,^{15}N-labeled $K[Au(CN)_2]$, the shape of which evinces the axial symmetry of the CS tensor. Also shown in Figure 2 are the specific effects of $R_{eff}(^{15}N,^{13}C)$, $\delta_{11} = \delta_{22}$, and δ_{33} on the spectrum.

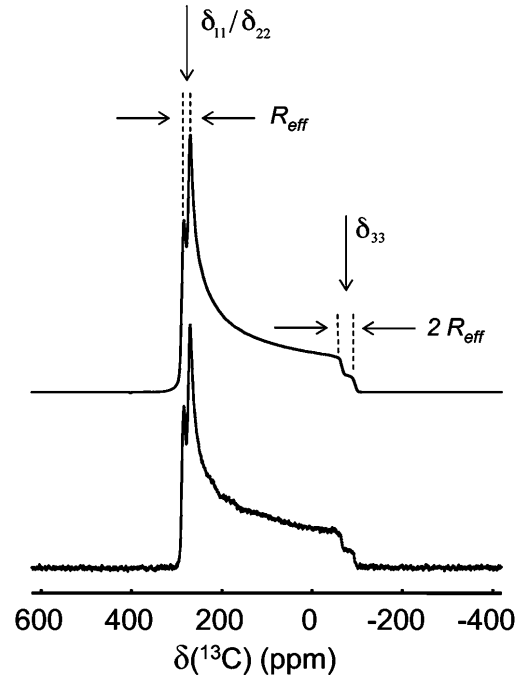

Figure 2. Simulated (upper trace) and experimental (lower trace) ^{13}C NMR spectra of a stationary sample of $K[Au(CN)_2]$ at 11.75 T.

The axial symmetry and principal component values of the CS tensor allow its orientation to be assigned as δ_{33} along the C−N bond, and the equivalent δ_{11},δ_{22} components perpendicular to the bond (vide infra). Parameters obtained from line shape simulations of the ^{13}C NMR spectrum from $K[Au(CN)_2]$ are presented in Table 2. After the vibrational corrections of $R_{eff}(^{15}N,^{13}C)$ described in section 2 were applied, a C−N distance of 1.15(4) Å was derived. This bond length is consistent with the X-ray-diffraction-derived value of 1.17(20) Å. The NMR-derived bond length is of higher precision than the X-ray value, whose lower than typical precision is probably due to the large electron density of the neighboring gold atom. This example shows how a SSNMR experiment can supplement an X-ray diffraction study where it may be difficult to pick out light atoms against a background of very heavy atoms.

The CS tensor for a carbon-13 nucleus in a linear molecule is defined by two components: $\delta_\perp$, measured perpendicular

(139) Bryce, D. L.; Bernard, G. M.; Gee, M.; Lumsden, M. D.; Eichele, K.; Wasylishen, R. E. *Can. J. Anal. Sci. Spectrosc.* **2001**, *46*, 46–82.
(140) Bak, M.; Rasmussen, J. T.; Nielsen, N. C. *J. Magn. Reson.* **2000**, *147*, 296–330.
(141) Ahrland, S.; Dreisch, K.; Norén, B.; Oskarsson Å. *Mater. Chem. Phys.* **1993**, *35*, 281–289.
(142) Pathaneni, S. S.; Desiraju, G. R. *J. Chem. Soc., Dalton Trans.* **1993**, 319–322.
(143) Jameson, A. K.; Jameson, C. J. *Chem. Phys. Lett.* **1987**, *134*, 461–466.

Table 2. Parameters Derived from Simulations of Carbon-13 SSNMR Spectra

salt	Au site	δ_{iso} (ppm)	LWHH[a] (Hz)	Ω (ppm)	κ	$R_{eff}(^{15}N,^{13}C)$[b] (Hz)	C−N bond[c] NMR (Å)	C−N bond X-ray (Å)
$K[Au(CN)_2]$		158.7(1)	85	360(2)	1	1850(100)	1.15(4)	1.17(20)
$[R_4N][Au(CN)_2]$[d]		151.90(5)	25	341(2)	1	1800(150)	1.16(5)	1.03(4)
$Tl[Au(CN)_2]$	1 or 2	167.5(4)	255	361(50)	1			
$Tl[Au(CN)_2]$	1 or 2	161.3(4)	315	352(50)	1			
$Tl[Au(CN)_2]$	3	151.7(2)	250	338(50)	1			
$Pb[Au(CN)_2]_2(H_2O)$[e]		167(1)		346	>0.95			
$Pb[Au(CN)_2]_2$[e]		173(1)		353	>0.95			
$K[Au(CN)_4]$		107.8(1)	110	337(3)	0.485(10)	1925(200)	1.14(6)	
AuCN[f]		154.1(5)	450	357(5)	1	1925(100)	1.14(4)	1.150(28)

[a] LWHH measured at 7.05 T. [b] From best-fit simulated spectra. [c] Corrected for vibrational effects (see text). [d] R = *n*-butyl. [e] SSNMR study from Katz et al.[38] [f] AuCN(B) as representative of the main site in all samples, see text.

to the long axis of the molecule, and $\delta_{||}$, measured along it; furthermore, it is well-known that $\delta_{||}$ will be approximately −90 ppm.[144,145] In brief, the reason for this is that $\sigma^{paramagnetic}$, the term responsible for most of the change in shielding between nuclei in differing environments, is identically zero along a C_∞ axis.[146] $K[Au(CN)_2]$ has CS tensor components $\delta_{11} = \delta_{22} = 279$ ppm and $\delta_{33} = -81$ ppm, but the orientation of the PAS cannot be determined from symmetry arguments because the molecule is not quite linear, see Table 1. However, the value of δ_{33} is similar enough to that expected for $\delta_{||}$ in a linear molecule to imply that it is oriented along the CN bond. The two remaining components, δ_{11} and δ_{22}, must therefore be perpendicular to the CN bond.

A relaxation study was also performed on $K[Au(CN)_2]$, at 4.70 T, in order to investigate the origins of the ^{13}C NMR peak's line width. The ^{13}C longitudinal relaxation time constant, $T_1 \simeq 5$ min, was measured using an inversion−recovery experiment in which 10 data points with delays of 121 μs to 1200 s were measured. The value of the transverse relaxation time constant, $T_2 \simeq 4.3$ ms, was measured using a 90°−τ−180°−τ−ACQ Hahn-echo pulse sequence, in which τ was increased from 0.25 to 10.90 ms in seven steps. For a Lorentzian line shape, the line width at half-height, LWHH, caused by T_2 is given by $(\pi \times T_2)^{-1}$; therefore, the LWHH of the potassium salt expected from T_2 relaxation alone is ∼ 75 Hz, close to the experimentally measured value of 85 Hz. It can therefore be concluded that residual dipolar coupling with ^{197}Au does not affect the ^{13}C spectrum, and ^{197}Au is probably self-decoupled because of efficient ^{197}Au quadrupolar relaxation at room temperature.

The structure of $[(n\text{-}C_4H_9)_4N][Au(CN)_2]$ differs from that of $K[Au(CN)_2]$ in that the $[Au(CN)_2]^-$ units are separated by large tetra-*n*-butylammonium cations,[75] with the closest Au−Au contact well beyond the reach of aurophilic bonding at 8.05 Å.[141,142] Local structural parameters for the single crystallographically independent site are provided in Table 1. The line width obtained for samples under MAS, 25 Hz, is much less than the value expected from residual dipolar coupling with ^{197}Au, see section 2; therefore, the quadrupolar nucleus is clearly self-decoupled at room temperature. Carbon-13 NMR parameters derived from theoretical simulation of experimental spectra from the 30% $^{13}C,^{15}N$-labeled material are given in Table 2. These spectral simulations show an axially symmetric CS tensor and a value of −75 ppm for δ_{33}. Following the reasoning from above, we assign an analogous CS tensor orientation, that is, δ_{33} along the C−N bond. The published value for the C−N bond length, 1.03(4) Å,[75] appears anomalously short when compared to typical values. Deriving a C−N bond directly from R_{eff} yields 1.194(33) Å, and after the vibrational corrections discussed above are applied, a final bond length of 1.16(5) Å is found. Whether correcting for vibrational effects or not, the NMR-derived values are more consistent with a typical C−N bond length than the 1.03(4) Å X-ray value. The most likely explanation for the discrepancy is the inherent difficulty of fitting the small C,N electron densities against the background of the large Au atom when analyzing the X-ray experiment. Further discussion of this C−N bond length is presented below.

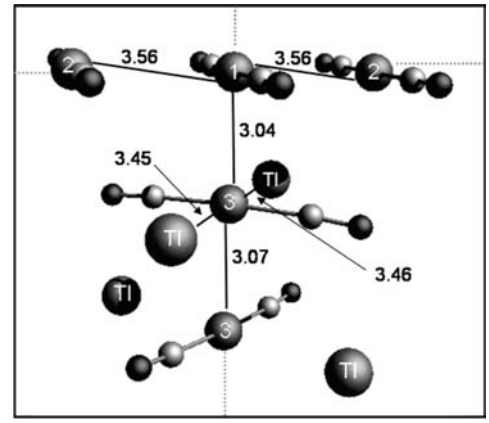

Figure 3. Local structure of $Tl[Au(CN)_2]$ depicting the intersection of the two Au chains, where Au atoms 1, 2, and 3 are numbered, and metallophilic bond lengths are given in Ångstroms. Cyanide ligands are oriented with carbon bonded to the gold atoms.

There have been several diffraction studies performed on the complicated $Tl[Au(CN)_2]$ structure,[77,147,148] in which there are gold−gold as well as gold−thallium metallophilic bonds. The unit cell is composed of alternating layers of Tl atoms and $Au(CN)_2$ groups; a small section of the unit cell is reproduced in Figure 3. There are three crystallographically distinct Au atoms, and these are linked together into two perpendicular chains of Au atoms with bond lengths as noted in Figure 3 and Table 1. There is an interesting range of Au

(144) Beeler, A. J.; Orendt, A. M.; Grant, D. M.; Cutts, P. W.; Michl, J.; Zilm, K. W.; Downing, J. W.; Facelli, J. C.; Schindler, M. S.; Kutzelnigg, W. *J. Am. Chem. Soc.* **1984**, *106*, 7672–7676.
(145) Dickson, R. M.; McKinnon, M. S.; Britten, J. F.; Wasylishen, R. E. *Can. J. Chem.* **1987**, *65*, 941–946.
(146) Ramsey, N. F. *Phys. Rev.* **1950**, *78*, 699–703.
(147) Fischer, P.; Ludi, A.; Patterson, H. H.; Hewat, A. W. *Inorg. Chem.* **1994**, *33*, 62–66.
(148) Fischer, P.; Mesot, J.; Lucas, B.; Ludi, A.; Patterson, H.; Hewat, A. *Inorg. Chem.* **1997**, *36*, 2791–2794.

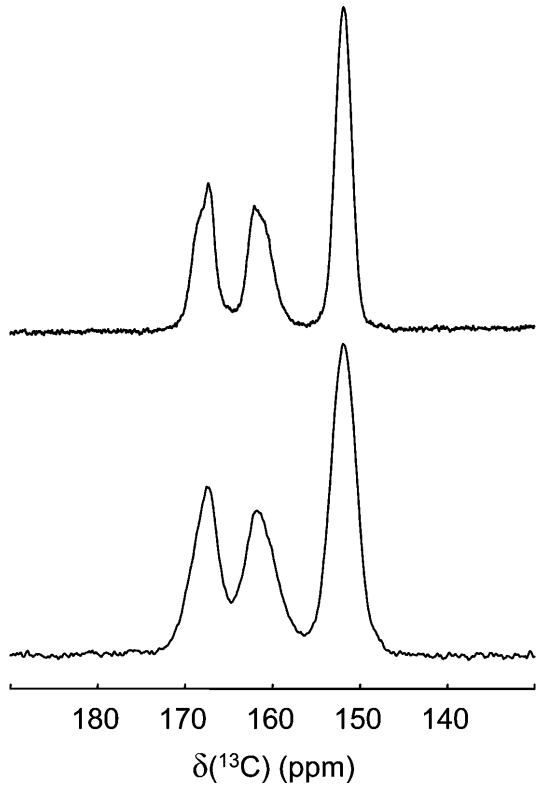

Figure 4. Upper spectrum: ^{13}C NMR spectrum of Tl[Au(CN)$_2$] under MAS, ν_{rot} = 12 kHz, acquired at 11.75 T. Lower spectrum: ^{13}C NMR spectrum of Tl[Au(CN)$_2$] under MAS, ν_{rot} = 10 kHz, acquired at 7.05 T.

coordination environments displayed in the structure: Au(1) shares bonds with four gold atoms, Au(2) is bound to two gold atoms, and Au(3) is coordinated to two gold and two thallium atoms. The two CN ligands bound to each Au atom are not related by any symmetry elements, so that there are a total of six distinct carbon atoms in the structure. In the following discussion, we label the two carbons bonded to Au(1) as C1 and C2, those bonded to Au(2) as C3 and C4, and those bonded to Au(3) as C5 and C6; the nitrogen atoms will be labeled analogously. The occurrences of Au(1) to Au(2) and Au(3) in the unit cell are in the ratio 1:1:2, and there is therefore the same total number of C5 and C6 atoms as there is for C1 through C4 atoms.

Spectra from 30% ^{13}C,^{15}N-labeled samples of Tl[Au(CN)$_2$] undergoing MAS are shown in Figure 4, where the 1:1:2 ratio of peak heights is apparent; it is interesting that the six symmetry-unique carbon atoms in Tl[Au(CN)$_2$] produce only three ^{13}C peaks in the MAS NMR spectrum at 7.05 T. In the analogous spectrum at 11.75 T, the two high-frequency peaks are asymmetric, which demonstrates that these two peaks arise from at least two carbon sites each. Given that at least four of the total six carbon sites are associated with the two high-frequency peaks, and that there must be twice the intensity produced from C5 and C6 as from C1−C4 sites, the only possible assignment is that the low-frequency peak is the sum of peaks from carbon atoms C5 and C6. It follows that the two high-frequency peaks are each composed of signals from one pair of the C1 through C4 atoms.

The structure of Tl[Au(CN)$_2$] provides valuable insight into the isotropic chemical shifts observed. The authors of the original neutron diffraction study noted that the observed *Pbcn* structure of Tl[Au(CN)$_2$] displays pseudosymmetry: all positions in the crystal deviate by at most 0.3 Å from a higher-symmetry *Imcb* structure.[77] In the higher-symmetry space group, C1 to C4 are all equivalent, and C5 is equivalent to C6. One point of note is that, within the *Pbcn* structure, Au(1) and Au(2) are differentiated by the fact that Au(1) is involved in an extra aurophilic bond, being at the intersection point of the two perpendicular Au chains shown in Figure 3. In the theoretical *Imcb* structure, Au(1) and Au(2) of the *Pbcn* structure converge to a single site, but only every second occurrence of the site equivalent to Au(3) from the *Pbcn* structure is occupied. This alternating occupation of Au(3) splits into two the otherwise equivalent C1 through C4 atoms in the *Imcb* structure. The pseudosymmetry reported by Blom et al.[77] demonstrates that the six nonequivalent carbon sites in the *Pbcn* structure are geometrically very close to being only three sites. It is also apparent from this argument that C1 through C4, shown above to be split into two NMR peaks 6.2 ppm apart, are different from each other in two ways: small geometrical differences and different aurophilic bonding of the directly bonded gold atom.

The pseudosymmetry present in Tl[Au(CN)$_2$] provides a hint that the presence of two distinct chemical shifts from carbons C1−C4 is due to the presence of the different arrangements of aurophilic bonds. However, the experimental structure contains deviations of up to 0.3 Å from the higher-symmetry *Imcb* structure, so it is necessary to explicitly compare the local structure around each carbon atom. The geometry of each Au(CN)$_2$ anion in the structure is strikingly similar: all bond lengths are equal within 0.003 Å, and all bond angles within 4.2° (see Table 1). Therefore, it seems unlikely that the local structure of each anion is responsible for producing the two different chemical shifts observed for C1−C4. The first coordination sphere around the Au(CN)$_2$ anions containing C1 to C4 includes thallium cations and neighboring Au(CN)$_2$ anions. It is important to evaluate the thallium contacts because this heavy atom can have a large effect on the chemical shift of nearby nuclei, an effect known as the relativistic heavy-atom light-atom (HALA) effect.[149,150] The HALA effect involves a relativistic induction of electron spin density on the heavy atom, the outcome being an altered chemical shift at nearby nuclei. The Au(CN)$_2$ anions containing C1−C4 are coordinated at each end by two Tl atoms, the average N−Tl bond length being 2.871 Å. While the Tl−N bond length is different for each nitrogen atom, the maximum deviation from this average is only 0.055 Å. It therefore seems unlikely that the very small changes in anion geometry and cation coordination are responsible for splitting the chemical shifts of C1−C4. We can then ascribe one of the two high-frequency peaks to C1 and C2, and the other peak to C3 and C4. The 6.2 ppm difference in

(149) Nomura, Y.; Takeuchi, Y.; Nakagawa, N. *Tetrahedron Lett.* **1969**, 639–642.

(150) Autschbach, J.; Ziegler, T. Relativistic Computation of NMR Shieldings and Spin-Spin Coupling Constants In *Encyclopedia of Nuclear Magnetic Resonance*; Grant, D. M., Harris, R. K., Eds.; John Wiley and Sons: Chichester, U.K., 2002; Vol. *9*, p 306.

chemical shifts between the two peaks provides a measure of the effect of the two 3.04 Å aurophilic bonds formed by the gold atoms bonded to C1 and C2, but not the gold atoms bonded to C3 and C4.

The low-frequency NMR peak of $Tl[Au(CN)_2]$ is assigned to carbons C5 and C6 as a corollary to the above arguments and is shielded by 15.8 and 9.6 ppm with respect to the two peaks from carbons C1 through C4. Insight into why the chemical shift for C5/C6 differs from the two chemical shifts for C1/C2 and for C3/C4 is again provided by consideration of the structure. This final $Au(CN)_2$ anion is also coordinated at the nitrogen atom by two thallium cations: N5 at 2.856 and 3.039 Å and N6 at 2.861 and 3.091 Å. There is also a third, more distant, N−Tl contact at 3.414 Å for N5 and 3.178 Å for N6. Given that these more distant thallium contacts are significantly different, but C5 and C6 have the same chemical shift, these longer Tl−N bonds are probably not too influential on the shift. The remaining distances are similar to the range of 2.816−2.904 Å N−Tl bond lengths of N1 through N4, but the deviations from average are slightly larger. Comparison of the $Au(CN)_2$ anion containing Au(3) to the anions containing Au(1) and Au(2) shows that the anion geometry is nearly identical and the thallium coordination to the nitrogen atoms is also similar; however, there is a significant difference in the metallophilic bonding environment at Au(3), where two Au−Au and two Au−Tl bonds are present (see Figure 3). This difference in metallophilic bonding is therefore assigned as the cause of the difference observed for the chemical shifts of carbon atoms C5/C6 as compared to those for C1 through C4. There are somewhat larger variations in local structure around C5 and C6 as compared to C1 through C4, namely, bond angles in the anion and N−Tl contacts, so assignment of the chemical shift change to solely alteration of the metallophilic bonding near C5 and C6 is less certain than for the case of C1 and C2 versus C3 and C4. However, the difference in metallophilic bonding in the anion is likely the dominant effect causing the different chemical shifts found for C5/C6 versus those of C1 through C4. In summary, a variation in isotropic ^{13}C chemical shifts of 6.2 ppm from differences in aurophilic bonding has been observed, while differences in metallophilic gold−thallium bonding have been found to cause a variation of 15.8 ppm.

The ^{13}C NMR spectrum of a stationary sample of $Tl[Au(CN)_2]$ was also acquired; unfortunately, multiple sites and broad line widths make deconvolving the line shape difficult. An axially symmetric CS tensor is expected from the investigation of $K[Au(CN)_2]$ and $[(n\text{-}C_4H_9)_4N][Au(CN)_2]$, and the line shape of this static spectrum is consistent with that symmetry. Therefore, a value of $\kappa = 1$ was fixed in the simulations. Spectral overlap prevented determination of the three R_{eff} values; the simulations instead used the average value of R_{eff}, 1815 Hz, from $K[Au(CN)_2]$ and $[(n\text{-}C_4H_9)_4N][Au(CN)_2]$. With the geometry, R_{eff}, δ_{iso}, and κ fixed, the only remaining parameter is the span, Ω. An initial estimate of Ω can be obtained from the fact that δ_{33} is not expected to change very much from −80 ppm (vide supra). For an axially symmetric CS tensor, $\Omega = 1.5\ (\delta_{iso} - \delta_{33})$, making initial estimates of the respective spans for the $\delta_{iso} = 151.7$, 161.3, and 167.5 ppm sites equal to 348, 362, and 371 ppm. A simulated spectrum using these parameters closely matches the shape of the experimental one but is slightly too broad. Reduction of each span by 10 ppm produced a theoretical spectrum matching well with the experimental one, and the chemical shift parameters are shown in Table 2. Because the three sites are not resolved, the entire width of the region containing the high-frequency discontinuites, ∼50 ppm, is reported as an error range. However, given the above arguments used to set the initial estimate of Ω, this large error range can be viewed as rather generous. A stationary experiment was chosen over a slow MAS experiment in order to limit the total MAS experimental time used for this thallium salt given its expected toxicity.

The ^{13}C MAS NMR spectrum of $Tl[Au(CN)_2]$ differs from those of the potassium and tetra-*n*-butylammonium aurocyanides in that a larger line width is observed, see Table 2. The observed line widths match well with the values predicted from coupling to the neighboring ^{197}Au nucleus, vide supra, but this is not the only possible source of line broadening. Other sources include chemical shift broadening, spin−spin coupling to $^{205/203}Tl$, or rapid relaxation. Comparing the line shapes of the two high-frequency peaks at 4.70 and 11.75 T shows that the two underlying sites are beginning to separate. In contrast, the line shape of the 151.7 ppm peak is nearly exactly superimposable despite the magnetic field strength more than doubling. Such a field-independent line width shows that the cause is not a distribution of chemical shifts, which would lead to superimposable peaks plotted on a parts per million rather than a frequency scale. We also performed relaxation measurements on $Tl[Au(CN)_2]$ to measure the ^{13}C T_1 and T_2 relaxation time constants of the 151.7 ppm sites using the same methods applied to $K[Au(CN)_2]$; however, the measurements on $Tl[Au(CN)_2]$ were performed at 11.75 T. The T_1 was determined to be ∼17 min, using nine data points spanning 1−1200 s. Hahn-echo experiments yielded T_2 as ∼7.3 ms, where the long T_1 limited acquisition to only four data points, spanning 0.15−10.05 ms (at which point the signal had decayed to <10% of its original value). In this case, the contribution from T_2 to the LWHH is only ∼45 Hz, whereas the experimental value of the LWHH is much larger at 250 Hz. Coupling with other nuclei in the sample is the only remaining explanation of the broad ^{13}C line width in $Tl[Au(CN)_2]$. However, it is not possible at this time to differentiate between coupling to the directly bonded ^{197}Au and $^{205/203}Tl$ nuclei. This ambiguity arises because, while one would expect $^{205/203}Tl$,^{13}C dipolar interactions to be removed by MAS, $J(^{205/203}Tl, {}^{13}C)$ would not be.

4.2. ^{15}N NMR of Gold(I) Dicyanides. The sample of 30% ^{13}C,^{15}N-labeled $[(n\text{-}C_4H_9)_4N][Au(CN)_2]$ discussed above was also investigated using ^{15}N SSNMR. A CP Hahn-echo spectrum from a stationary powder of this sample together with the best-fit simulation is displayed in Figure 5, while data determined from spectral simulations are given in Table 3. Just as in the ^{13}C data, an axially symmetric ^{15}N CS tensor

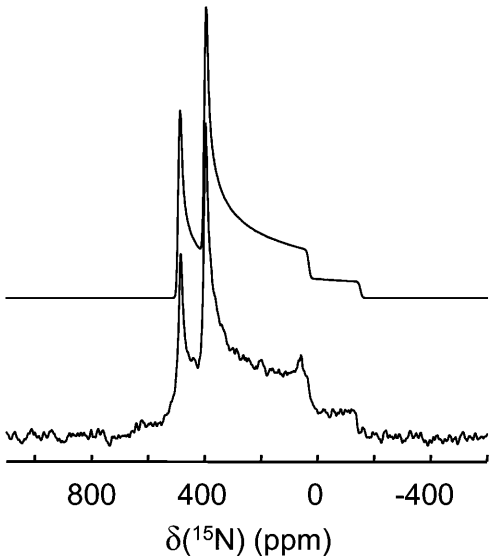

Figure 5. Simulated (upper trace) and experimental (lower trace) ^{15}N cross-polarized NMR spectra of a stationary sample of $[(n\text{-}C_4H_9)_4N][Au(CN)_2]$ at 4.70 T.

is found, so the orientation of δ_{33} is assigned as coincident with the C−N bond. The derived value of R_{eff}, 1790(75) Hz, agrees with the value determined from the ^{13}C spectrum within experimental uncertainty. Correcting for vibrational effects leads to a final bond length of 1.17(3) Å. Both NMR measurements of R_{eff}, by observing ^{13}C or ^{15}N, support the value of a typical C−N bond length, in opposition to the X-ray study, where an anomalously short distance was reported.

The sample of 50% ^{13}C,^{15}N-labeled K[Au(CN)$_2$] was also studied using ^{15}N SSNMR; however, the long T_1 values and lack of protons for CP enhancement prevented acquisition of spectra from stationary samples. Values for the CS parameters were therefore obtained from a slow-spinning MAS experiment. As mentioned above, the spinning-sideband intensities depend on the CS tensor span and skew, as well as the dipolar coupling to the neighboring ^{13}C nucleus. The spinning sideband intensities were analyzed as an AX spin pair using the nonlinear least-squares fitting mode of the SPINEVOLUTION software package.[110] The value of R_{eff}(^{15}N,^{13}C) used in this analysis was fixed to that found from analysis of the ^{13}C NMR spectrum, and the orientation of δ_{33} was not varied but affixed along the C−N bond axis. Presented in Figure 6 is the experimental spectrum and best-fit simulation, while the parameters used in the simulation are given in Table 3. Error values shown in Table 3 are 99% confidence intervals determined in the fitting procedure. However, the procedure does not incorporate error values in the experimental peak heights, so the reported error values should be considered conservative. Also, for isolated spins, the difficulty in obtaining accurate values of κ from slow MAS data in systems where this parameter is near 1 has been well documented,[94,97] and this difficulty probably persists in the present AX spin system. The fact that the fitting procedure determines a value of approximately 1 for κ, and reports a small error range, should therefore not be overinterpreted in terms of being an absolute determination of axial symmetry.

Nitrogen-15 NMR spectra of Tl[Au(CN)$_2$] were also acquired. The isotropic peak of the MAS spectrum is displayed in Figure 7, where it may be observed that none of the six unique cyanides are clearly resolved. Unfortunately, the low receptivity of ^{15}N combined with the broad lines and site multiplicity prevented determination of the CS tensors from slow MAS experiments. If the hypothesis that ^{13}C chemical shifts of Tl[Au(CN)$_2$] are insensitive to small changes in local geometry but dependent mainly on bonding around the Au atom is correct, the further-displaced ^{15}N nuclei would be expected to show less sensitivity in their chemical shifts. Conversely, if it were the thallium contacts that instead controlled the ^{13}C chemical shifts, the ^{15}N nuclei would be expected to display a larger spread in chemical shifts, as they are all closer to the Tl atoms. The above assignment of metallophilic bonding controlling ^{13}C chemical shifts is thus borne out in the observation of clearly separated ^{13}C peaks, while nonequivalent ^{15}N sites remain unresolved.

4.3. ^{13}C and ^{15}N NMR of a Gold(III) Tetracyanide. A sample of 50% ^{13}C,^{15}N-labeled potassium tetracyanoaurate-(III), K[Au(CN)$_4$], was prepared in order to investigate how the formal oxidation number of Au affects the cyanide NMR parameters. A structure for the hydrate has been published,[151] but we found the dehydrate more amenable to NMR study, as the hydrate is not stable to dehydration[131] and also yielded fewer NMR resonances than expected for the low-symmetry hydrate. Neutron diffraction data for the hydrate evidence an approximately square-planar [Au(CN)$_4$] anion, no Au−Au contacts < 4.8 Å, and bond lengths similar to those of the gold(I) cyanides.[151] For an ideal D_{4h} [Au(CN)$_4$] anion, two of the mirror planes would restrict the principal axis systems of both ^{13}C and ^{15}N CS tensors: one component would be along the CN bond, one perpendicular to the plane of the molecule, and the third perpendicular to the first two components.

Only one ^{13}C isotropic peak is observed in the MAS NMR spectrum for the unknown dehydrate structure, evidencing a close similarity to D_{4h} symmetry. We therefore expect the CS tensor to have an orientation similar to that described for a D_{4h} tetracyanoaurate anion. When the spectrum of a stationary sample is observed, Figure 8, it is clear that the value of δ_{33} is very similar to that observed for the gold(I) dicyanides. This similarity provides further evidence that one CS tensor component is aligned along the C−N bond and allows assignment of that component as δ_{33}. Therefore, the value of β was assigned as 0°, which allowed the best-fit simulated spectrum displayed in Figure 8 to be generated, using the parameters reported in Table 2. The remaining task is to assign which of the principal CS tensor components is perpendicular to the (approximate) molecular plane. When δ_{11} and δ_{22} are compared, it may be seen that the value of δ_{11}, 246 ppm, is similar to the ~270 ppm found for δ_{11} and δ_{22} values in the dicyanoaurate(I) salts, while the value of δ_{22}, 162 ppm, is quite different. This comparison to the

(151) Bertinotti, C.; Bertinotti, A. *Acta Crystallogr., Sect. B* **1970**, *26*, 422–428.

Table 3. Parameters Derived from Simulations of Nitrogen-15 SSNMR Spectra

salt	δ_{iso} (ppm)	LWHH[a] (Hz)	Ω (ppm)	κ	$R_{eff}(^{15}N,^{13}C)$[b] (Hz)	C−N bond[c] NMR (Å)	C−N bond X-ray (Å)
$K[Au(CN)_2]$	266.0(1)	25	475(20)	0.993(4)			
$[R_4N][Au(CN)_2]$[d]	275.33(5)	9	505(5)	1	1790(75)	1.17(3)	1.03(4)
$Tl[Au(CN)_2]$	291.3(5)	325					
$Tl[Au(CN)_2]$	284(2)	325					
$Pb[Au(CN)_2]_2(H_2O)$[e]	266(1)		480	>0.8			
$Pb[Au(CN)_2]_2(H_2O)$[e]	259(1)		450	>0.7			
$Pb[Au(CN)_2]_2$	276(1)						
$K[Au(CN)_4]$	285.31(5)	25	495(25)	1.000(1)			
$K[Au(CN)_4]$	282.38(5)	25	495(30)	0.989(1)			
AuCN[f]	224.0(4)	275	425(25)	1			

[a] LWHH measured at 11.75 T. [b] From best-fit simulated spectra. [c] Corrected for vibrational effects (see text). [d] R = *n*-butyl. [e] SSNMR study from Katz et al.[38] [f] AuCN(B) as representative of the main site in all samples, see text.

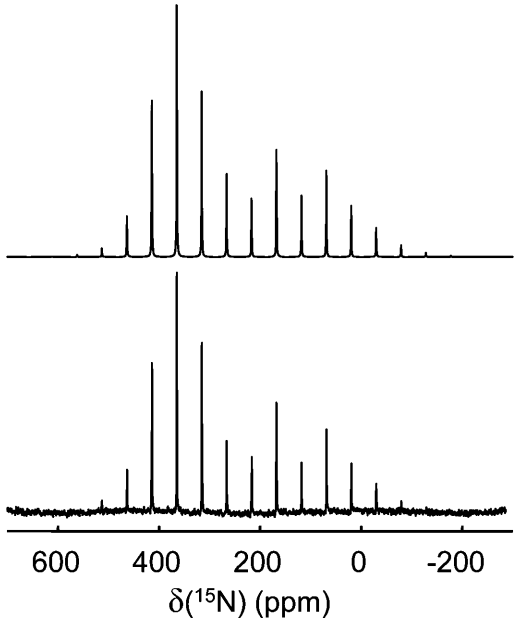

Figure 6. Simulated (upper trace) and experimental (lower trace) slow-spinning ^{15}N NMR spectra of $K[Au(CN)_2]$ at 11.75 T (ν_{rot} = 2.5 kHz).

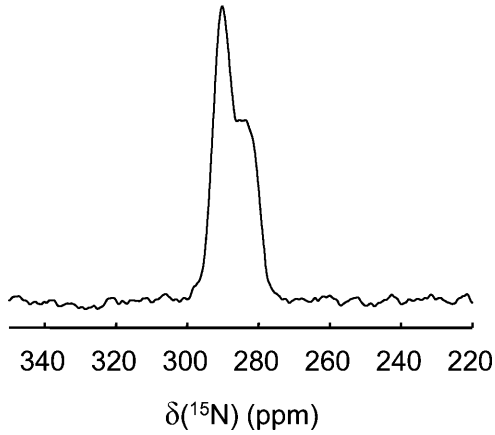

Figure 7. Experimentally observed ^{15}N NMR spectrum of $Tl[Au(CN)_2]$ at 11.75 T under MAS (ν_{rot} = 10 kHz).

gold(I) dicyanides shows that δ_{22} is the component out of the molecular plane, as CS tensor components are sensitive to changes in the planes perpendicular to their direction. The $[Au(CN)_4]$ anion may not be of D_{4h} symmetry, so the described tensor orientation should be taken as approximate. However, given the similarity of $\delta_{33} = -88$ ppm to the value of ∼−80 ppm observed for the gold(I) dicyanides, it seems unlikely that δ_{33} deviates much from the C−N bond vector.

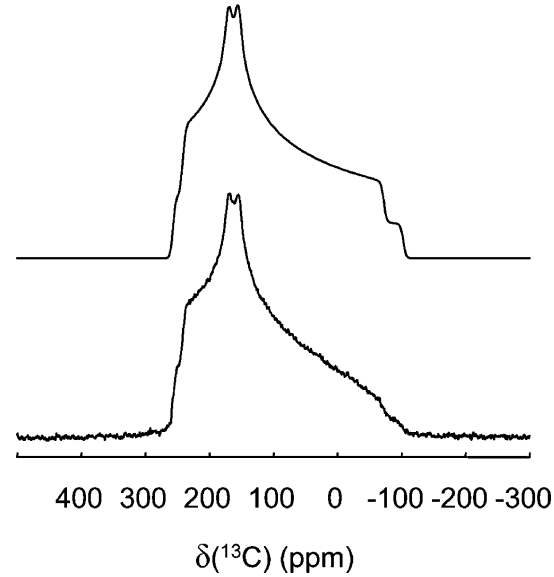

Figure 8. Experimental (lower trace) and simulated (upper trace) ^{13}C NMR spectra of a stationary sample of $K[Au(CN)_4]$ at 11.75 T.

Nitrogen-15 NMR data for the 50% ^{13}C,^{15}N-labeled sample of $K[Au(CN)_4]$ are summarized in Table 3. The CS tensors for each of the two sites were determined using the same method applied for analysis of $K[Au(CN)_2]$: nine peaks from a slow MAS spectrum obtained at 11.75 T were modeled as an AX spin system using a least-squares fitting method.[110] Again, the value of R_{eff} was fixed to the value determined from the ^{13}C NMR spectrum, and δ_{33} was affixed along the C−N bond vector. There are two isotropic ^{15}N shifts observed, showing that the dehydrate crystal structure may deviate at least somewhat from anions of D_{4h} symmetry. It is perhaps worthwhile pointing out that the presence of two ^{15}N peaks does not prove a break from D_{4h} symmetry, since there may simply be two molecules in the asymmetric unit cell of this unknown structure. However, the small 2.9 ppm difference in isotropic shifts would not require much deviation from D_{4h} symmetry. While the ^{13}C isotropic shift for this gold(III) cyanide lies some distance from the observed range of values for gold(I) cyanides, the ^{15}N isotropic shift of $K[Au(CN)_4]$ lies within the range seen for gold(I) complexes. The carbon atom is directly bound to the gold atom, and hence its chemical shift is affected greatly by a change in oxidation state of the metal. The more distant

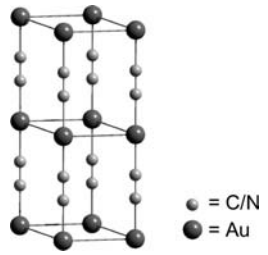

Figure 9. Two unit cells of AuCN; carbon and nitrogen atoms are not distinguished by the neutron diffraction experiment and are therefore represented using the same shade. See text for further discussion of the structure.

nitrogen atom has its chemical shift less affected by the oxidation state of the metal, less in fact than the differences in bonding and geometry between dicyanoaurate(I) anions in different salts.

4.4. ^{13}C NMR of Gold(I) Monocyanide. AuCN is an interesting material that resisted structural characterization for a long time due to the unavailability of crystals suitable for single-crystal diffraction measurements. A combined total neutron diffraction and X-ray diffraction study of the powdered material determined the structure but showed evidence of disorder.[82] The structure is depicted in Figure 9, where it can be seen that the infinite ···CN−Au−CN··· chains are aligned to form sheets of aurophilically bonded Au atoms (Au−Au distance = 3.39 Å). Interestingly, one phase of AuCN monolayers adsorbed on a Au(111) surface has been shown, through scanning tunneling microscopy and low-energy electron diffraction, to have the same structure as a 2D slice of the structure displayed in Figure 9.[152,153] An alternative AuCN structure has also been proposed in the literature and investigated using DFT;[154,155] however, no evidence for this theoretical polymorph was observed in the powder X-ray diffraction patterns recorded here. While a structure of AuCN was obtained in the diffraction studies,[78,82] the equivalence of the Au−C and Au−N bond lengths in AuCN makes it impossible to determine the orientation of the cyanide ligand in the chains from diffraction experiments alone. The chain structures of CuCN and AgCN have been shown via NMR and NQR evidence to contain disordered CN vectors;[86,87] therefore, it is likely that "head−tail" cyanide disorder also exists in AuCN. Reported error parameters from the neutron diffraction data fitting procedure suggest that there may be some slipping of the chains, i.e., the weak aurophilic bond is broken so that some neighboring chains do not align at the gold atoms.[82] There are of course other types of disorder, for example, vacancies, that can occur in such systems, but the two varieties described above are the most likely.

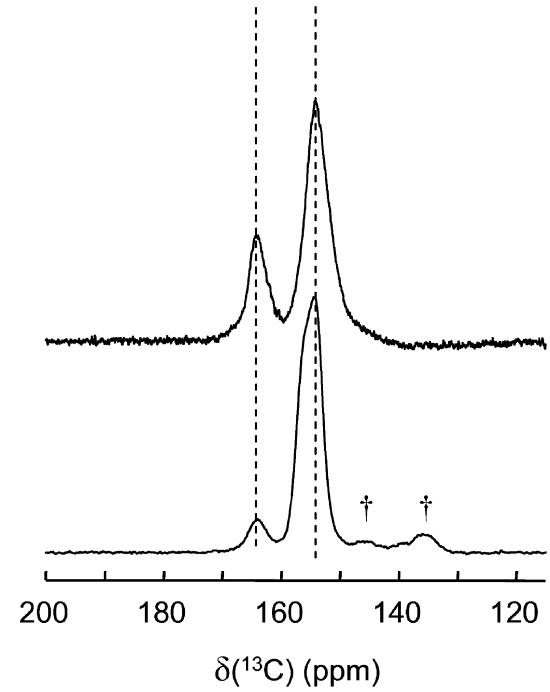

Figure 10. Upper spectrum: ^{13}C NMR spectrum of AuCN(A) under MAS, ν_{rot} = 13 kHz, acquired at 11.75 T. Lower spectrum: ^{13}C NMR spectrum of AuCN(B) under MAS, ν_{rot} = 10 kHz, also acquired at 11.75 T. Peaks marked with a † in the spectrum of AuCN(B) have been assigned as impurities (see text).

Table 4. Carbon-13 NMR Parameters of AuCN

AuCN sample	δ_{iso} (ppm)	LWHH[a] (Hz)	area (%)
AuCN(A)	154.1(5)	590	76
	164.1 (5)	450	24
AuCN(B)	154.6(5)	545	84
	164.0(5)	450	6.5
	136(2)	540	6.5
	145(2)	650	3

[a] LWHH measured at 11.75 T.

Figure 10 shows the MAS spectrum of AuCN(A), while the isotropic shifts, line widths and area are summarized in Table 4. There are two isotropic shifts visible despite the fact that the crystal structure contains only one unique site in the absence of disorder. A 2D homonuclear dipolar-recoupling experiment, $SR26_4^{11}$, was performed in order to determine if there was an impurity or if there was indeed two different sites in the material. The ∼5 ms excitation period used yield spectra sensitive to ^{13}C,^{13}C dipolar couplings corresponding to C−C distances of ∼5 Å, the exact distance depending on complicated experimental and site parameters. This distance is large enough that, even under the presence of chain slipping and CN head−tail disorder, intersite correlation can be probed. In the $SR26_4^{11}$ experiment, peaks occur only for dipolar-coupled nuclei and are observed in the indirect dimension at the sum of the chemical shifts for the two sites. The format of the experimental spectrum shown in Figure 11 is such that the self-correlation peaks expected from the network structure of AuCN occur on the diagonal and are observed for both peaks. Because the two sites are at +10 and +20 ppm from the transmitter in the direct dimension, the two +30 ppm peaks in the DQ dimension demonstrate intersite connectivity. Experimental

(152) Sawaguchi, T.; Yamada, T.; Okinaka, Y.; Itaya, K. *J. Phys. Chem.* **1995**, *99*, 14149–14155.
(153) Yamada, T.; Sekine, R.; Sawaguchi, T. *J. Chem. Phys.* **2000**, *113*, 1217–1227.
(154) Hakala, M. O.; Pyykkö, P. *Chem. Commun.* **2006**, 2890–2892.
(155) Zaleski-Ejgierd, P.; Hakala, M.; Pyykkö, P. *Phys. Rev. B: Condens. Matter Mater. Phys.* **2007**, *76*, 094104.
(156) The samples used in the 2002 study were still present in our lab, and a check of their IR spectra revealed a single resonance for each of the 99% labeled samples (dilabeled ^{13}C, ^{15}N as well as monolabeled ^{15}N and ^{13}C materials).

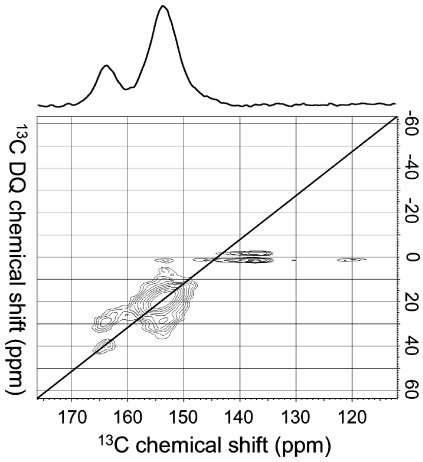

Figure 11. Carbon-13 $SR26_4^{11}$ homonuclear dipolar-recoupling spectrum of AuCN(A) acquired under MAS, ν_{rot} = 9.615 kHz, at 11.75 T. The spectrum resulted from 6 days of experimental time. The corresponding 1D Bloch-decay experiment is placed at the top of the spectrum. In the presented expansion, self-correlation appears on the diagonal, while intersite correlations occur as pairs of peaks off the diagonal. Spectral artifacts have no frequency dependence in t_1 and occur at 0 ppm in the indirect dimension.

artifacts have no frequency dependence in the second dimension and create the small features at 0 ppm. Unfortunately, the similarity of model C−C distances produced by head−tail disorder or chain slipping precluded us from attempting to distinguish between them at the resolution available using this experiment.

Two separate ^{13}C isotropic shifts are observed within the same material; therefore, the chemical shift of the carbon nucleus must be sensitive to some disorder in the material. Assignment of the multiplicity as due to head−tail cyanide disorder or chain slipping can be performed by comparison to the expected chemical shift effect of each. In a SSNMR study of CuCN, an upper limit of ∼2 ppm for the difference in $\delta_{iso}(^{13}C)$ from a change in neighboring CN orientation was found; that is, the difference in δ_{iso} for ^{13}C−Cu−NC versus ^{13}C−Cu−CN is <2 ppm.[86] The analogous effect of cyanide orientation on the ^{13}C chemical shift in the material AgCN was placed as approximately 0.8 ppm.[87] The carbon−metal bond distance in AuCN is midway between that of AgCN and CuCN, so the effect of neighboring CN orientation on the ^{13}C chemical shift is likely midway between 0.8 and <2 ppm, or at least much less than 10 ppm. Because chain slipping would be accompanied by the breaking of aurophilic bonds, the effect of chain slipping on $\delta_{iso}(^{13}C)$ can be estimated from the data presented above for $Tl[Au(CN)_2]$. For $[Au(CN)_2]^-$ moieties with nearly identical geometries, changes are seen in the ^{13}C isotropic shifts of up to 15.7 ppm because of the difference in the metal identity and length of metal−metal bonds, while a change of 5.9 ppm was observed for differences in the number and length of Au−Au contacts for aurophilic bonding. The observed 10 ppm difference between the two AuCN(A) sites is consistent with this range while being noticeably larger than the small range expected from CN head−tail disorder. This argument does not rule out the presence of head−tail disorder; it simply shows that any effect of that type of disorder on $\delta_{iso}(^{13}C)$ is likely hidden in the large (5 ppm) line width.

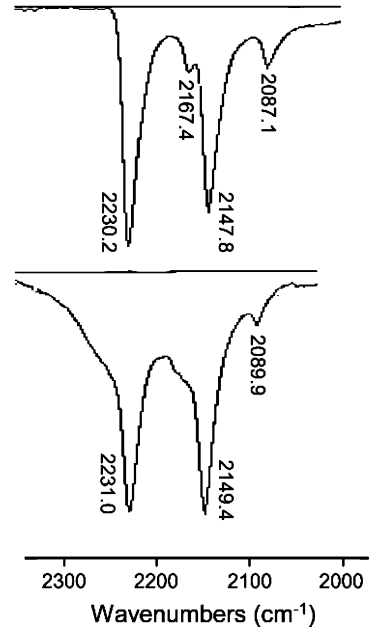

Figure 12. IR spectra of the CN stretching region, upper spectrum from AuCN(A) and lower spectrum from AuCN(B)

Infrared spectroscopy is also useful and serves to confirm the interpretation of the ^{13}C NMR spectra from this material. The infrared spectrum of AuCN(A), represented in Figure 12, shows two ^{12}C,^{14}N peaks at 2230.2 and 2167.4 cm^{-1}, which have a similar intensity ratio to those in the ^{13}C NMR spectrum. Two peaks from the ^{13}C,^{15}N-labeled cyanides in the sample are also visible at 2147.8 and 2087.1 cm^{-1}, positions matching well with those predicted by the simple harmonic oscillator model. Sensitivity of the IR spectrum to head−tail disorder versus chain slipping may be found by investigating the analogous material AgCN. NMR spectroscopy has shown that there is head−tail cyanide disorder in AgCN, while there is only one stretch present in the IR spectrum.[87,156] It seems that vibrational spectroscopy is not sensitive to head−tail disorder, perhaps because the M−C versus M−N force constants mimic the indistinguishability of the bond lengths. In the silver-based material, without aurophilic bonding, the chains are farther apart than those in AuCN at 5.9 versus 3.4 Å and are not aligned at the metal position. Since the chains of AuCN interact more strongly than those of AgCN, it is quite plausible that IR spectroscopy is sensitive to chain slipping in AuCN, while no change is observed in AgCN. Vibrational spectroscopy therefore supports the ^{13}C NMR argument for the presence of chain slipping in AuCN.

An alternate synthetic method, vide supra, yielded AuCN(B), whose ^{13}C NMR spectrum, powder XRD pattern, and IR spectrum provide further insight into the AuCN system. Two samples were synthesized using this method, and the two samples were found to produce nearly exactly superimposable ^{13}C line shapes at 11.75 T. The ^{13}C NMR spectrum of AuCN(B) is shown in Figure 10, with the corresponding line shape information in Table 4. This second sample has two additional peaks beyond the pair of resonances in common with AuCN(A). When the ^{13}C SSNMR spectra for the two samples are compared, it may be seen

that the ratio of the pair of resonances the two samples have in common differs; there is more of the high-frequency site in AuCN(A). A sample with more chain slipping would be expected to yield a broader XRD pattern, whereas a sample with a differing amount of head−tail disorder would yield the same XRD peak breadths due to the similar scattering power of C and N atoms. Line widths in the XRD pattern of AuCN(B) are narrower than those from AuCN(A), consistent with an assignment of the 154 ppm site as an ordered site and the 164 ppm peak as a chain slipped site.

Unfortunately, lower intensity and resolution prevented the use of an $SR26_4$[11] experiment to identify the extra two peaks in the ^{13}C NMR spectrum of AuCN(B). The nature of the sites producing these two NMR resonances is, however, hinted at by the XRD pattern of AuCN(B): if the extra peaks represented new types of disorder superimposed on the AuCN structure, an XRD pattern broader than that observed for AuCN(A) would be expected, whereas a narrower pattern is observed. On the other hand, amorphous impurities could very easily cause only a broad, diffuse X-ray pattern and not provide any noticeable change in the overall XRD pattern. We therefore assign the two low-frequency ^{13}C NMR peaks of AuCN(B) as amorphous impurities rather than components in a disordered AuCN structure. The IR spectrum of AuCN(B), represented in Figure 12, contains the same peaks as the spectrum from AuCN(A), but the CN region is broader. Such an increased breadth of IR resonances from AuCN(B) is also consistent with the presence of amorphous impurities in that sample. Identification of the low-frequency peaks as impurities also seems logical, as it is unlikely that AuCN(B), which has less chain slipping, would be the material that displays an increase in the types of disorder. Investigation of a second sample with a slightly different composition yielded observations entirely consistent with the above assertion of measurable chain slipping in AuCN. Interestingly, the 7 ± 2% fraction of cyanides in slipped chains observed for AuCN(B) is lower than the 24 ± 5% found for AuCN(A).

In an effort to investigate the synthesis used to prepare AuCN(A), a second material, AuCN(A′), was prepared with a different amount of reducing agent. Synthesis of AuCN(A) used less than a stoichiometric amount (75%) of the reducing agent and was found to yield a sample that contained a very broad ^{13}C resonance centered at ∼50 ppm to low frequency of the main peaks. We assign this broad peak as cyanides bound to Au(III) from the isotropic shift observed for $K[Au(CN)_4]$. The approximately 30-ppm-broad (at 11.75 T) peak was found to remain even after the washing process. Use of a small (10%) excess of the reducing agent produced AuCN(A′), in which some of the Au(III) ions from solution were reduced further than to the intended target of Au(I). Comparison of the XRD pattern to that of a Au(s) powder showed that there was indeed some metallic gold present. The presence of Au(s) also affected the color of the material: the expected lemon yellow color was found to be tinted green. Clearly, batches of AuCN made via the process in patent #4,222,996[132] without careful control of the amount of reducing agent will contain either Au(III) or Au(0) as an impurity. The two samples AuCN(A) and AuCN(A′) were found to contain the same percentage of cyanides assigned to slipped chains, 24 ± 5% and 25 ± 5%, respectively.

On the basis of the above analysis of the spectra from MAS samples, we feel the two isotropic shifts displayed by AuCN are well understood; however, the broad line shapes are complicated and require further experiments to fully understand. The pair of isotropic shifts displayed in the spectra of AuCN(A) result from chain-aligned and chain-slipped sites, but the width of these two peaks probably has a contribution from varying numbers of aurophilic bonding partners, as well as from head−tail cyanide disorder. The line width of the 154 ppm peak of AuCN(A), see Table 4, is approximately 30% smaller in hertz at 7.05 T versus 11.75 T; this smaller line width at lower applied field is consistent with the presence of a distribution of chemical shifts, which could result from disorder in the number of aurophilic bonding partners as well as head−tail cyanide disorder. Comparing the 154 ppm peaks of AuCN(A) and AuCN(B) at 11.75 T shows that the two have nearly the same line width, where the only significant difference is that the peak from AuCN(B) is slightly narrower at the base. However, the 154 ppm peak of AuCN(B) does not display the same narrowing in hertz upon decreasing the applied field. Instead, this peak is nearly exactly superimposable when plotted on a frequency scale at 7.05 and 11.75 T, so that it is wider than the corresponding peak in AuCN(A) at 7.05 T. The behavior of the 154 ppm peak from AuCN(B) with changing field points to some field-independent broadening mechanism, see above for further discussion of the possibilities, but it is unusual that this mechanism seems to be absent, or at least lessened, in AuCN(A). Perhaps some difference in T_2 relaxation time constants or in residual dipolar coupling with ^{197}Au causes the discrepancy between the two samples. However, further experiments would be required to address this matter properly. One possible method would be to apply annealing techniques, shown useful in diffraction studies of CuCN,[80] to remove some of the disorder-induced chemical shift broadening of this peak, or to use high-temperature experiments to decouple ^{197}Au in order to separate the line broadening mechanisms.

The ^{13}C NMR spectrum from a stationary sample of AuCN(B), see Figure 13, has the appearance of that from a single-site material. Most likely, the powder pattern is representative of the 85% dominant site, see Table 4, with the other minor sites contributing to broadening only. Simulation of this powder pattern therefore provides the CS tensor and $R_{eff}(^{15}N,^{13}C)$ coupling constant from the main, aligned-chain, site. If we ignore cyanide head−tail disorder in neighboring chains, a factor unlikely to affect the CS tensor, the CN bond lies along a C_6 symmetry axis.[82] Therefore, the CS tensor is axially symmetric, and the PAS is oriented with δ_{33} along the C−N bond.[89,95,96] Parameters from the best-fit simulation are given in Table 2, where it may be seen that the 1.14(4) Å C−N bond length agrees well with the neutron-diffraction value of 1.150(28) Å.

4.5. ^{15}N NMR of Gold(I) Monocyanide. Nitrogen-15 NMR of AuCN was also investigated. The MAS spectrum

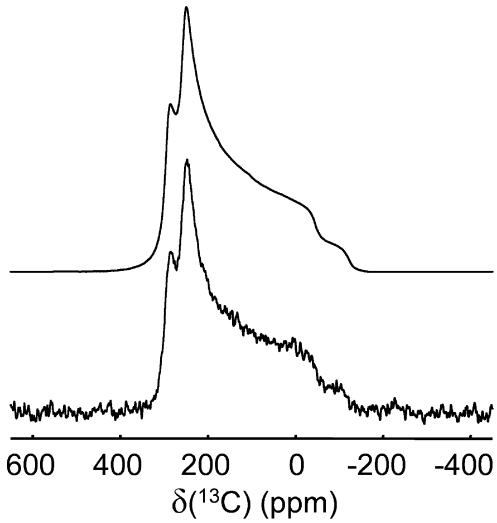

Figure 13. Experimental (lower trace) and simulated (upper trace) ^{13}C NMR spectra of a stationary sample of AuCN(B) at 4.70 T.

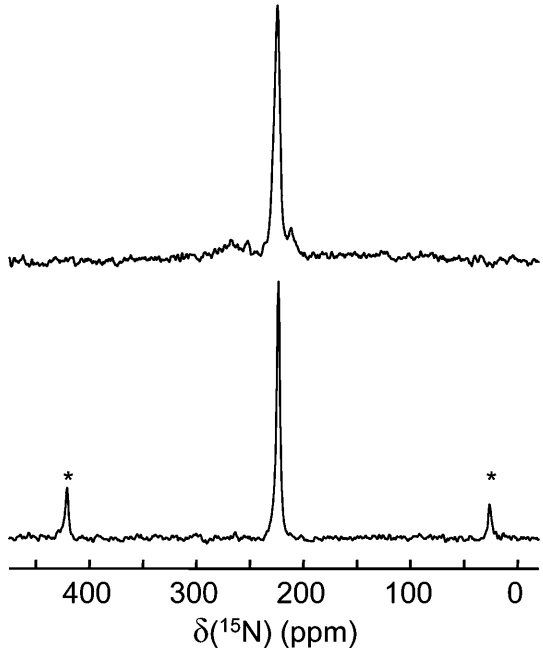

Figure 14. Upper spectrum: ^{15}N NMR spectrum of AuCN(A) under MAS, $\nu_{rot} = 13$ kHz, acquired at 11.75 T. Lower spectrum: ^{15}N NMR spectrum of AuCN(B) under MAS, $\nu_{rot} = 10$ kHz, also acquired at 11.75 T.

Table 5. Nitrogen-15 NMR Parameters of AuCN

AuCN sample	δ_{iso} (ppm)	LWHH[a] (Hz)	area (%)
AuCN(A)	224.1(5)	300	87
	211.5(10)	300	6
	370(10)	1500	7
AuCN(B)	223.40(25)	200	100

[a] LWHH measured at 11.75 T.

of AuCN(A), shown in Figure 14, is nearly ninety percent one resonance, with a small peak to low frequency and a broad absorbance to high frequency, see Table 5. Nitrogen-15 chemical shifts are typically more sensitive to environmental changes than are carbon-13 shifts, which hints at one possible explanation for the spectrum seen in Figure 14. While only two distinct values are observed for $\delta_{iso}(^{13}C)$, for aligned and shifted chains, the more sensitive ^{15}N nucleus may allow resolution of more sites, e.g., differences in the number of nearest neighbors. If the argument about increased sensitivity for ^{15}N over ^{13}C is the true cause of the increased number of sites, it may be that increased chemical shift broadening is responsible for the lower relative integrated intensity of the secondary peaks in the ^{15}N spectrum (see data for AuCN(A) in Table 4 versus that in Table 5). Also shown in Figure 14 is the nitrogen-15 spectrum of AuCN(B) under MAS, an interesting spectrum in that only one peak is visible despite the multiplicity seen in the carbon-13 spectra. AuCN(B) has less than one-third the amount of slipped chains as does AuCN(A), which may be the reason that secondary resonances are only observed in nitrogen-15 spectra of the latter. Particularly given that the ^{15}N NMR spectra of AuCN(A) display secondary resonances at only approximately half the integrated intensity seen in the ^{13}C NMR spectra of this material. We did attempt to observe secondary peaks in a ^{15}N spectrum of AuCN(B) by increasing the applied field to 21.14 T (a 91.2 MHz Larmor frequency), but only a single peak was obtained.

There is some uncertainty in a full assignment of the ^{15}N data, but there is little doubt that the main $\sim$ 224 ppm resonance is that of the neutron-diffraction structure (i.e., aligned gold cyanide chains). This peak is the same in all the samples, so we used the highest-quality slow MAS spectrum, that of AuCN(B) at 11.75 T, to determine the ^{15}N CS tensor; the results are reported in Table 3. Eight peaks from the experimental spectrum were used in the least-squares fit,[110] and R_{eff} was set to the value determined from the ^{13}C NMR spectrum. Due to the C_6 symmetry axis at the nitrogen,[82] the model used for analyzing the spectrum had κ fixed to 1, and δ_{33} fixed along the C−N bond. The ^{15}N chemical shift of AuCN lies outside the range found for those from the other gold(I) and gold(III) cyanides presented above. As might be expected, $\delta_{iso}(^{15}N)$ appears more sensitive to the formation of a new bond directly to nitrogen in this bridging CN ligand, than to the small geometry changes between gold(I) dicyanides or even to the change in oxidation state of the gold atom. Previously reported nitrogen-15 data from a dicyanoaurate in which the cyanide forms a bridging bond to lead in $Pb(H_2O)[Au(CN)_2]_2$ (and its dehydrate),[38] see Table 3, exhibits ^{15}N chemical shifts that match better with the range observed here for nonbridging cyanide groups than that observed for the bridging cyanide of AuCN. The reason for the $\delta_{iso}(^{15}N)$ of $Pb[Au(CN)_2]_2(H_2O)_x$ agreeing better with the nonbridging nitrogen environments may be that the Pb−N bond is much longer (2.595−2.8 Å) than the Au−N bond in AuCN (1.9703 Å).

5. Conclusions

Carbon-13 and nitrogen-15 NMR spectra of several gold(I) dicyanides and one gold(III) tetracyanide have been acquired and are useful in providing survey data for the interpretation of future NMR experiments on cyanoaurate coordination polymers. Chemical shift tensors for the cyano ^{13}C and ^{15}N nuclei are reported, and a range of isotropic shifts for the various environments are determined. Static ^{13}C, and in some cases ^{15}N, NMR spectra are used to provide several r(C,N) distance measurements and allow a value of 1.17(3) Å for

the C−N bond in $[(n\text{-}C_4H_9)_4N][Au(CN)_2]$, more accurate than the existing X-ray diffraction measurement, to be determined. The impact of metallophilic bonding on ^{13}C chemical shifts is isolated, and this bonding is found to cause a range of approximately 16 ppm in $\delta_{iso}(^{13}C)$. Also, the influence of gold's formal oxidation state on ^{13}C and ^{15}N chemical shifts are determined.

The disordered material AuCN was investigated by studying several samples using ^{13}C and ^{15}N NMR, powder X-ray diffraction, and IR spectroscopy. Homonuclear carbon-13 dipolar recoupling experiments are found to be invaluable in determining whether NMR peaks arise from the same or differing materials. Furthermore, the ^{13}C isotropic chemical shift is found to be sensitive to alignment of the one-dimensional chains with respect to their neighboring chains, that is, breaking of the aurophilic bonds.

Carbon-13 and nitrogen-15 NMR experiments provide a clearer picture of the disorder superimposed on the average structures of the coinage metal monocyanides. These materials are all composed of one-dimensional ···NC−M−CN··· chains,[78−85] and $^{65/63}Cu$ NQR studies in combination with ^{13}C and ^{15}N NMR spectroscopy of CuCN and AgCN have shown that the orientation of the cyanide ligands varies: 30 ± 10% of the metal sites were disordered (C−M−C or N−M−N), while 70 ± 10% were ordered (C−M−N).[86,87] Disorder of the cyanide orientations is likely also present in AuCN but simply not visible given that the expected effect on the chemical shifts is smaller than the observed line widths. The major difference between the structures of AuCN and CuCN/AgCN is that, with the presence of gold, there is an increased interaction between the metal atoms. Because only very weak interactions between the chains in CuCN and AgCN exist, any misalignment of the chains creates no visible effect on the NMR parameters. It follows logically that the stronger interchain forces in AuCN allow the possibility of chain slipping to be investigated. The amount of this disorder in AuCN is found here to vary with the synthetic method, the two syntheses applied here producing samples containing from 7 ± 2% to 25 ± 5% slipped chains. It is likely that the lowered strength of interchain interactions in AgCN/CuCN versus AuCN is responsible for an increased amount of chain slipping in the two lighter systems. This increased slipping is consistent with the broader XRD patterns observed for AgCN/CuCN as compared to AuCN.[78] The body of research on the group 11 monocyanides all converges to describe a picture of these materials as infinite one-dimensional chains, with a significant fraction of the cyanide ligands disordered and also with a large percentage of the chains slipped with respect to their neighbors.

Acknowledgment. The authors thank the solid-state NMR research group at the University of Alberta for many helpful discussions. Professor David Bryce, University of Ottawa, is also thanked for his interest in this project, as well as the acquisition of spectra from initial gold cyanide samples. We also thank Dr. Victor Terskikh, Canadian National Ultrahigh-Field NMR Facility for Solids, for acquisition of spectra at 21.14 T. The National Ultrahigh-Field NMR Facility for Solids (Ottawa, Canada), is a national research facility funded by the Canada Foundation for Innovation, the Ontario Innovation Trust, Recherche Québec, the National Research Council Canada, and Bruker BioSpin and managed by the University of Ottawa (www.nmr900.ca). The Natural Sciences and Engineering Research Council of Canada (NSERC) supports operation of this facility through a Major Resources Support grant. Dr. Darren Brouwer, NRC Steacie Institute for Molecular Sciences, is also thanked for introducing us to the $SR26_4^{11}$ experiment, and for helpful discussions. Funding for this research was provided by the Natural Sciences and Engineering Research Council of Canada, as well as the Canada Research Chairs Program (R.E.W. holds a Research Chair in Physical Chemistry at the University of Alberta). K.J.H. also thanks the Province of Alberta for financial support, as well as the University of Alberta for initial funding of this research.

IC8022198